Division 2, National Defense Research Committee
of the
Office of Scientific Research and Development

THE EFFECT OF AIR BURST ON THE BLAST FROM BOMBS AND SMALL CHARGES

II. Analysis of Experimental Results

by

R. R. Halverson

NDRC Report No. A-320
OSRD Report No. 4899

Division 2, National Defense Research Committee
of the
Office of Scientific Research and Development

THE EFFECT OF AIR BURST ON THE BLAST FROM BOMBS AND SMALL CHARGES

II. Analysis of Experimental Results

by

R. R. Halverson

NDRC Report No. A-320
OSRD Report No. 4899

Submitted by Paul C. Cross

P. C. Cross, Research Director
Underwater Explosives Research Laboratory

Approved on April 6, 1945
for submission to the Committee E B. Wilson Jr

E. B. Wilson, Jr., Chief
Division 2
Effects of Impact and Explosion

The NDRC Technical Reports Section
for armor and ordnance edited
this report and prepared it for duplication.

Requests for additional copies should be
addressed through liaison channels to:
National Defense Research Committee
Technical Reports Section
Room 4724, Munitions Building
Washington 25, D.C.

Preface

The work described in this report is pertinent to the project designated by the Navy Department Liaison Officer as OD-03. The report constitutes a progress report under Contract OEMsr-569 with the Woods Hole Oceanographic Institution.

The empirical analysis of shock-wave reflection phenomena reported here represents satisfactorily the nature of the blast waves from air or groundburst charges for conditions thus far investigated experimentally. A simple procedure is presented for the prediction of shock configurations and of optimum heights of burst for peak pressure and for positive impulse under conditions for which no experimental data are available. This work should constitute a significant contribution toward the efficient use of the enhanced blast effect of air-burst bombs under appropriate circumstances.

E. B. Wilson, Jr.

Initial distribution of copies of the report

Nos. 1 to 17 to Liaison Office, OSRD;

Nos. 18 to 25 to Office of the Executive Secretary, OSRD;

No. 26 to R. C. Tolman, Vice Chairman, NDRC;

No. 27 to J. P. Baxter, III, Historian, OSRD;

Nos. 28 and 29 to E. B. Wilson, Jr., Chief, Division 2;

No. 30 to W. Bleakney, Deputy Chief, Division 2;

No. 31 to M. P. White, Technical Aide, Division 2;

No. 32 to H. L. Bowman, Member, Division 2;

No. 33 to W. E. Lawson, Member, Division 2;

No. 34 to D. P. MacDougall, Member, Division 2;

No. 35 to S. A. Vincent, Member, Division 2;

No. 36 to J. von Neumann, Member, Division 2;

Nos. 37 and 38 to Division 2 Library, Princeton University;

Nos. 39 and 40 to Office of Field Service (J. E. Burchard, V. V. Sides);

No. 41 to Ordnance Department Liaison Officer with NDRC;

Nos. 42 to 49 to Bureau of Ordnance [Research and Development Division (2 copies), Lt. Comdr. S. Brunauer, A. Wertheimer, P. C. Keenan, R. J. Seeger, J. A. Weyl, Comdr. J. A. E. Hindman];

Nos. 50 to 53 to Aberdeen Proving Ground (Ballistic Research Laboratory, Maj. J. S. Lieb, R. H. Kent, R. G. Sachs);

Nos. 54 to 64 to Liaison Office, OSRD, for Division 2 London Representative; H. P. Robertson; Road Research Laboratory; Armament Research Department; Ministry of Home Security; Lt. Col. J. W. Berretta (2 copies); J. MacNeille; W. B. Mann; G. T. Young; Dorothy Weeks;

No. 65 to Army Ground Forces Liaison Officer with NDRC;

Nos. 66 and 67 to David Taylor Model Basin (Comdr. J. Ormondroyd, E. H. Kennard);

No. 68 to Picatinny Arsenal (Technical Group);

Nos. 69 to 76 to Ordnance Department (Col. R. G. Butler, Col. C. H. M. Roberts, Col. I. A. Luke, Lt. Col. G. C. Tibbetts, S. Feltman, J. E. Levy, L. R. Littleton, H. M. Morse);

Nos. 77 and 78 to Corps of Engineers (Lt. Col. S. B. Smith, C. Beck);

No. 79 to Engineer Board (Maj. C. A. Burress);

No. 80 to Engineer Board Experiment Station (Capt. T. F. Adams);

No. 81 to R. D. Huntoon, Office of the Secretary of War;

Nos. 82 and 83 to AAF Board, Orlando, Fla. (President; S. S. Cairns);

Nos. 84 and 85 to Joint Target Group (Lt. Comdr. W. W. Timmis);

Nos. 86 and 87 to Eglin Field, Fla. (Col. S. P. Huff, Lt. L.R. de Alva);

No. 88 to Target Analysis Section, Joint Intelligence Center, Pacific Ocean Area (Lt. Comdr. T. C. Wilson);

No. 89 to Director, Air Technical Service Command, Wright Field, Dayton, Ohio (TSESE-4I);

No. 90 to Office of Coordinator of Research and Development, Navy Department (Comdr. R. D. Conrad);

No. 91 to Army Air Forces (Lt. Col. J. M. Gruitch);

Nos. 92 and 93 to Bureau of Ships (Capt. H. G. Rickover, Comdr. C. H. Gerlach);

Nos. 94 to 103 to Operations Analysis Division, Management Control, HQ, AAF;

Nos. 104 to 106 to War Department Liaison Officer with NDRC for transmittal to Col. P. Schwartz, Air Ordnance Officer European Theater; L. A. Brothers and Col. W. G. de Steiguer, Operations Analysis Division 20 AF;

No. 107 to Th. von Kármán, Director, Scientific Advisory Group, HQ, AAF;

No. 108 to New Developments Division, War Department (Lt. Col. H. S. Turner);

No. 109 to Assistant War Department Liaison Officer with NDRC (Lt. Col. W. P. Allis);

No. 110 to Col. W. S. Bowen, Chairman's Office, NDRC;

No. 111 to A. Ellett, Chief, Division 4, NDRC;

No. 112 to R. A. Connor, Chief, Division 8, NDRC;

No. 113 to G. B. Kistiakowsky, Member, Division 8;

No. 114 to Thomas Bardeen, Gulf Research and Development Company;

No. 115 to J. A. Hornbeck, Land Mines Committee, NDRC;

No. 116 to H. C. Hottel, Member, Section 11.2, NDRC;

No. 117 to Mina Rees, Technical Aide, Applied Mathematics Panel;

No. 118 to P. C. Cross, Consultant, Division 2;

No. 119 to J. G. Kirkwood, Consultant, Division 2;

No. 120 to C. W. Lampson, Consultant, Division 2;

No. 121 to N. M. Newmark, Consultant, Division 2;

No. 122 to V. Rojansky, Consultant, Division 2;

No. 123 to A. H. Taub, Consultant, Division 2;

No. 124 to H. J. Fisher, Explosives Research Laboratory, Bruceton;

No. 125 to Explosives Research Laboratory Files;

No. 126 to W. D. Kennedy, Woods Hole Oceanographic Institution;

No. 127 to R. R. Halverson, Woods Hole Oceanographic Institution;

No. 128 to L. G. Smith, Princeton University.

CONTENTS

List of Figures

THE EFFECT OF AIR BURST ON THE BLAST FROM BOMBS AND SMALL CHARGES

II. Analysis of Experimental Results

Abstract

The experimental study of the effect of air burst carried out at the Underwater Explosives Research Laboratory has been reported in Part I of the progress report of this title (OSRD-4246) as well as in other papers (see list of references at the end of this report).

In the present report, an empirical method of analyzing and extending these data has been developed by expressing the data in terms of the angular variables of the theory of oblique, regular reflection.

In the first section of this report, the geometry of the Mach reflection phenomenon has been studied with particular reference to the path followed by the triple point (see Table I). An empirical curve was drawn [Fig. 8(a)] from which it is possible to express the height of the triple point as a function of the horizontal distance from the charge for any charge height and for any charge weight [Fig. 9(a)]. A study of the time interval at many gauge positions between the incident and reflected shocks gave the necessary information for drawing this curve. High-speed motion pictures of shocks from 500-lb GP bombs in which the Mach configuration could be seen (Fig. 11) were also used.

In the second section the pressure data are analyzed in a similar manner, and predictions are made as to the pressure distribution with charge height at gauge positions not studied experimentally.

In the third section the relation is studied between the charge height to maximize the pressure or impulse at a given gauge, and the charge height that causes the triple point to pass through that gauge position. From this correlation and by use of the results of the first section, the optimum charge height for pressure or impulse can be predicted.

I. GEOMETRY OF THE REFLECTION PHENOMENON

1. Geometry of reflection of plane, step shocks

Von Neumann[3/] has shown that the reflection of a plane, step shock wave from a rigid surface is "regular" for sufficiently small angles of incidence α. This regular reflection system consists of two shocks, the incident and

---

3/ This and all subsequent references are to the List of References at the end of this report.

reflected shocks [I and R, Fig. 1(a)]. For an incident shock of given strength ξ, there is an $\alpha_{extreme}$ such that for $\alpha > \alpha_{extreme}$ the regular reflection phenomenon is no longer possible, and must be replaced by some more complex system.

A system that is hydrodynamically possible for the case $\alpha > \alpha_{extreme}$ is the Mach shock system [Fig. 1(a)], which is nonstationary and composed of three shocks and a density discontinuity (slip stream), S.[3] That such a shock system exists has been demonstrated photographically (see, for example, Ref. 4). Here the reflected shock is not formed at the reflecting surface but at the tip of a high-pressure region called the Mach region, the front of which is called the "stem." The intersection M (triple point) of the incident shock, reflected shock, and slip stream moves away from the reflecting surface following a straight-line path $\ell - \ell$ as the phenomenon grows. In this shock system, the reflected shock R is no longer straight, nor is it a step shock as is the case in regular reflection.

2. Geometry of reflection of spherical, decaying shocks

That the same types of reflection occur in the case of a decaying spherical shock has likewise been demonstrated photographically (see Sec. 4 of present report and Ref. 5). In Fig. 1(b), the cases of regular and Mach reflection for spherical incident shocks are drawn, and the notation to be used in this report is indicated. It should be mentioned that in Fig. 1(b), the stem is drawn as vertical. It was drawn in this manner because calculations based on this configuration are carried out in the second section of this report. In actuality, the stem should be ahead of the spherical incident shock extended through the Mach region. A tabulation of all notation used in this report is given in Table I. (For experimental arrangement and data analyzed in this report, see Refs. 1 and 2.)

3. Study of reflection times for calculation of height of stem

In order to interpret the results obtained in the detonation of the three series of small bare charges (2-lb, 12-lb, and 40-lb TNT) and the three bomb series (500-lb, 1000-lb, and 2000-lb GP TNT and Composition B bombs) reported in Ref. 1 plus a recent series of 4.15-lb bare charges

Table I. Summary of notation used.

Notation	Meaning
h_c	Charge height, reduced to basis of 1 lb TNT (see Ref. 1 and Sec. 3)
h_g	Gauge height, reduced to basis of 1 lb TNT
I	Incident shock front.
R	Reflected shock front.
Stem	Shock front of Mach region (Mach shock).
S	Slip stream.
M	Triple point, intersection of I, R, S, and stem.
ℓ-ℓ	Locus of M.
D	Horizontal coordinate measured from charge, reduced to basis of 1 lb TNT.
D_o	Horizontal coordinate of point at which M would leave ground if Mach reflection began at $\alpha = \alpha_{extreme}$, reduced to basis of 1 lb TNT.
y	Vertical coordinate measured from ground, reduced to basis of 1 lb TNT.
r	Airline distance from the charge to any given point, reduced to basis of 1 lb TNT.
ξ	Ratio of absolute pressure before incident shock to that behind.
α	Angle between horizontal and tangent to incident shock at point of reflection.
α_1	Angle between horizontal and tangent at the ground to incident shock extended through the Mach region ($\alpha_1 = \alpha$ when $\alpha < \alpha_{extreme}$).
$\alpha_{extreme}$	Angle of incidence α at $D = D_o$, $y = 0$ (function of h_c only).
ϕ	Angle between horizontal and chord from $(D_o,0)$ to (D,y).
χ	Angle between horizontal and tangent to ℓ-ℓ at any point on ℓ-ℓ.
Reflection time	Time interval between arrival of incident and reflected shocks at the gauge, reduced to basis of 1 lb TNT.
P_P	Peak pressure of incident shock for gauge outside of Mach region (double-peak record, Fig. 8, p. 19, Ref. 1).
P_A	Minimum pressure before second peak on double-peak record.
P_R	Peak pressure of reflected or second shock on double-peak record.
P_i	Pressure of incident shock at time reflected shock arrives at gauge.

Table I. [Concluded.]

Notation	Meaning
P_r	$P_R - P_A + P_i$ = pressure rise in second shock plus pressure of incident shock at time reflected shock arrives at gauge. (This corresponds to the pressure behind the reflected shock for comparison with the theory for step shocks.)
R_{gM}	Distance along chord of reflected shock from M to point on reflected shock which hits the gauge, reduced to basis of 1 lb TNT.
P_M	Peak pressure of Mach shock measured by gauge within Mach region (single-peak record).
P_F	Pressure that would have been recorded by gauge within Mach region if there had been no reflection (free-air pressure, taken from smoothed pressure-distance curve).
τ	Apparent linear time-decay constant [= $(P_P - P_A)$/Reflection time], a function of both P_P and reflection time (reduced to basis of 1 lb TNT).

in which gauges were used at very small heights above the ground,[2] the pressure-time records were studied with a view to obtaining information concerning the geometry of the Mach phenomenon. The "reflection time," the time interval between arrival of the incident and reflected shocks at the gauge, was measured on the records obtained from the seven series and was scaled down to the basis of 1 lb TNT by dividing by the cube root of the charge weight (cf. Sec. III, Ref. 1). No account was taken of the case effect of the bombs (Sec. VII, Ref. 1). All linear distances were also scaled by the weight factor. In the rest of this report, therefore, all data will refer to a charge weight of 1 lb TNT, and to change to any charge weight W it is only necessary to multiply linear distances and times by $W^{1/3}$. To take into account case effect on pressure of a bomb, an additional factor can be applied to the $W^{1/3}$ factor.

From these data, plots were made of reflection time versus gauge height at a series of small ranges of charge height, and of reflection time versus charge height at a series of small ranges of gauge height for the two horizontal charge-to-gauge distances, D = 10.4 ft and D = 15.9 ft. Some data were also obtained for a horizontal charge-to-gauge distance D = 39.8 ft

(Figs. 2 through 5). In Fig. 4 are plotted the data from the recent series of 4.15-lb bare charges in which the gauges were placed at points very near the ground at a reduced horizontal distance of ~15.9 ft.[2] Note that the gauge-height scales are in inches for Figs. 4(b), 4(c), and 4(d). Both types of curves were extrapolated to zero reflection time in a manner to give a consistent family as well as to fit the experimental points plotted. The curve of Fig. 4(a) [data from the high, or "monitor" gauge] was extrapolated in a manner to be consistent with the family of curves of Fig. 3(a). The gauge height corresponding to a charge height that just produces a zero reflection time gives the vertical coordinate y of the triple point M for that charge height at the given value of D. From these data plots of stem height y versus charge height h_c at D = 10.4 ft and at D = 15.9 ft were drawn [Figs. 6(a) and 6(b)].

An additional point can be calculated for each of the curves of Figs. 6(a) and 6(b). That is, the values of charge height which give values of ξ and α such that $\alpha = \alpha_{extreme}$ at y = 0 and D = 10.4 ft and 15.9 ft, were calculated, and indicated on the curves of Figs. 6(a) and 6(b), respectively, as the theoretical limits of regular reflection.

The theoretical horizontal limit of regular reflection, D_o, was calculated for several values of charge height, and is plotted against charge height in Fig. 7. Also included on this curve at integral values of charge height are the values of $\alpha_{extreme}$ as defined in Table I. The calculation of D_o was carried out by use of a pressure-distance law, $P = 3.25(15.9/r)^{1.5}$, where P (lb/in^2) is the peak pressure at a distance r (ft) from a 1-lb TNT charge,[2] and by use of the curves of Polachek and Seeger[6] which give $\alpha_{extreme}$ as a function of ξ, the ratio of absolute pressure before the incident shock to that behind. In using these curves, the assumption is made that a decaying spherical shock being reflected from a rigid surface undergoes transition to Mach reflection under the same conditions of overpressure and angle of incidence as a plane step shock encountering a "corner."

It is seen from Fig. 6 that even for charge heights somewhat less than that corresponding to $D_o = D$ for each of the two curves, the height of the stem is zero. It is felt there is little question that these curves

are drawn correctly at the lower values of stem height, at least for D = 15.9 ft, because of the large amount of data obtained at very low gauge heights for that horizontal distance. These curves indicate that the Mach phenomenon does not set in for a spherical shock until some point beyond $\alpha_{extreme}$. This result is in qualitative agreement with that obtained in the Princeton shock tube.[8]

By knowing D_o as a function of charge height (Fig. 7) and by using the curves of Fig. 6, $\underline{\phi}$ (see list of definitions, Table I) can be calculated for D = 10.4 ft and D = 15.9 ft for various values of charge height. The value of $\underline{\alpha}$ (list of definitions, Table I) was calculated for these charge heights and these two values of $\underline{D}$. A tabulation was also made of $\alpha_{extreme}$ for these values of charge height (Fig. 7). In this way a series of corresponding values of $\underline{\phi}$, $\underline{\alpha}$, and $\alpha_{extreme}$ was obtained. A plot was then made of $\underline{\phi}$ versus $\alpha - \alpha_{extreme}$ [Fig. 8($\underline{a}$)]. It may be noted from this plot that there is no significant systematic difference between the values of $\underline{\phi}$ calculated from values of $\underline{y}$ at D = 10.4 ft and those calculated from values of $\underline{y}$ at D = 15.9 ft. In spite of the fact that this is not conclusive proof that the $\underline{\phi}$ versus $\alpha - \alpha_{extreme}$ curve is independent of the value of $\underline{D}$ from which it was computed, the assumption was made that this is true, since it was then possible to compute $\ell - \ell$, the locus of the triple point $\underline{M}$, for various values of h_c. Additional justification for this assumption is presented in Figs. 8($\underline{b}$), 9($\underline{b}$), 9($\underline{c}$), 10, and 11, which are discussed below.

From Fig. 8($\underline{a}$), the locus of $\underline{M}$ in terms of the linear coordinates $\underline{y}$ and $\underline{D}$ can be computed for a series of charge heights as follows. A series of corresponding values of $\underline{\phi}$ and $\alpha - \alpha_{extreme}$ is picked from the curve of Fig. 8($\underline{a}$). Then, for a given charge height, the values of D_o and $\alpha_{extreme}$ are obtained from Fig. 7. With these data the equations,

$$\tan \alpha = \frac{D}{h_c - y}, \qquad (1)$$

$$y = (D - D_o) \tan \phi, \qquad (2)$$

can be solved for the values of $\underline{D}$ and $\underline{y}$ for this series of points. This gives the locus of $\underline{M}$ for the given charge height. The results of these calculations for several integral values of charge height are plotted in Fig. 9($\underline{a}$).

4. Comparison of results with other sources of data

In order to compare the results of this calculation procedure with the experimental data obtained at the Princeton University Station, on a study of $\frac{1}{2}$-lb TNT blocks,[7] the foregoing procedure was carried out for values of $h_c = 2.91$, 4.31, 5.46, 7.56, and 9.35 ft. These results are plotted in Fig. 9(b) together with the Princeton curves for these values of h_c. The Princeton experimental points obtained by an extrapolation of reflection time data similar to those used here are included. It may be noted in Fig. 9(b) that the agreement between the two sets of curves is in most cases as good over the whole range of D for which Princeton has experimental points as it is at D = 10.4 ft and D = 15.9 ft, the two values of D for which extensive data are reported here. This fact is felt to be some justification for the assumption that the explicit dependence of ϕ on D is very slight.

The points for the smooth curve of Fig. 10, height of stem versus charge height at D = 39.8 ft, were obtained from the family of curves of Fig. 9(a) by reading the ordinates y at D = 39.8 ft for the various values of charge height. Included in Fig. 10 are four experimental points obtained from extrapolation of reflection time data (Fig. 5). It may be seen that the agreement between these points and the smoothed curve is very good, thus showing that the values of y at 39.8 ft as predicted by the data at 10.4 ft and 15.9 ft agree very well with those actually obtained. A theoretical point from Fig. 7 is also included on this figure.

Some additional justification for the assumption that the ϕ versus $\alpha - \alpha_{extreme}$ curve is independent of the value of D at which it was calculated was obtained from high-speed motion picture photographs ($\sim$2500 frames/sec) of the Mach configuration. These photographs were taken by W. E. Curtis during a recent series of blast measurements on 500-lb GP bombs detonated at a reduced charge height of 0.4 ft.[12] The triple point could be observed for a few frames at a reduced value of D of about 3.6 ft. Typical frames in which the triple point could be observed are reproduced in Fig. 11. In the following sketch is shown the Mach configuration as it is seen in the photographs of Fig. 11.

Values of ϕ and $\alpha - \alpha_{extreme}$ were calculated for these photographically determined positions of the triple point, and these data are plotted in

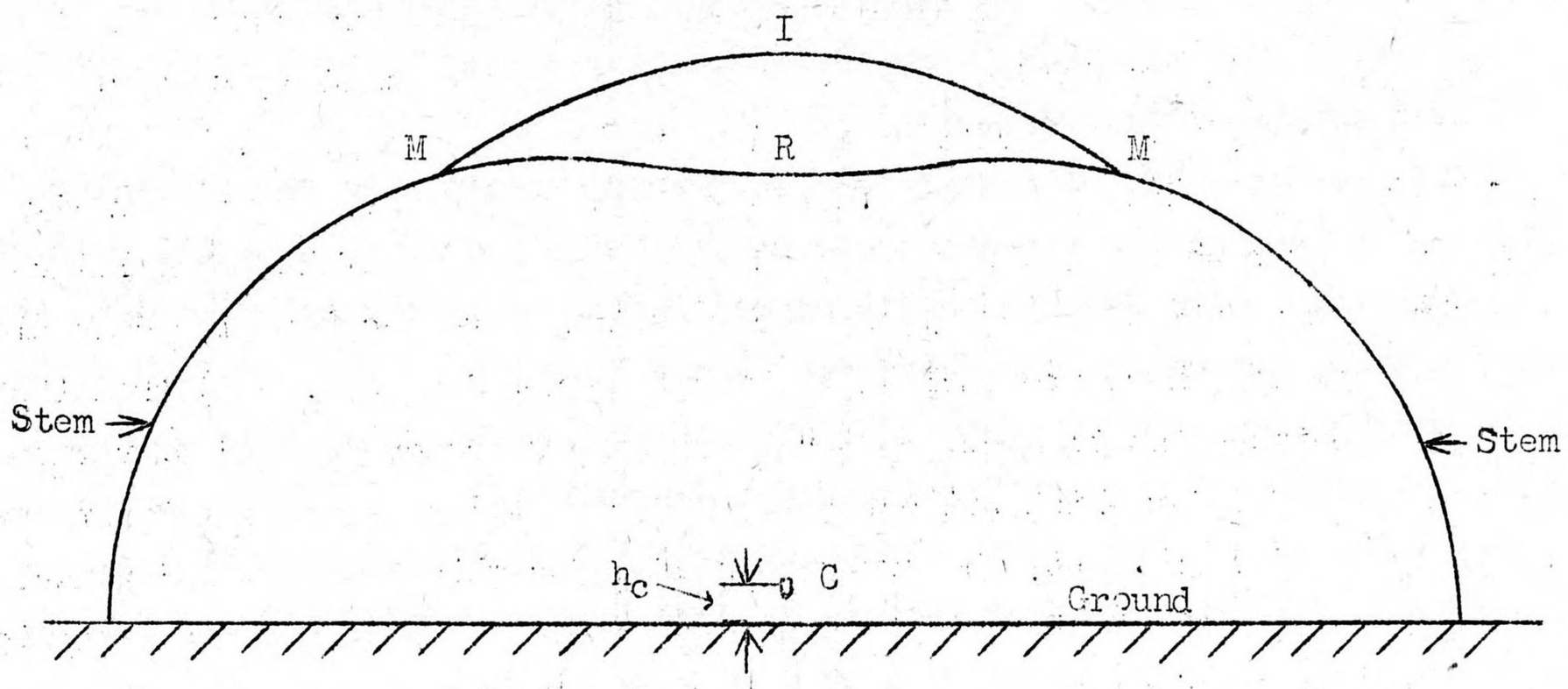

Fig. 8(b). The smoothed curve from Fig. 8(a) is also included in Fig. 8(b). It is seen that the photographically determined data fall on a reasonable extension of the curve determined from reflection time data. However, since in the limit $h_c = 0$, $D_o = 0$, Eqs.(1) and (2) degenerate into $\tan \alpha = -\cot \phi$, which holds for any point (D,y), the precision of this curve ($\underline{\phi}$ versus $\alpha - \alpha_{extreme}$) for predicting a triple-point path is not great for low values of h_c. Because of this fact, the scatter of experimental data in Fig. 8(b) is greatly compressed.

To show more clearly, however, that the photographic data do satisfy the empirical curve relating $\underline{\phi}$ and $\alpha - \alpha_{extreme}$, the $\ell - \ell$ locus was calculated for a reduced charge height of 0.4 ft by use of Fig. 8(b) with its extension through the photographic data. This locus is plotted in Fig. 9(c) together with the curves for $h_c = 2$, 3, and 4 ft taken from Fig. 9(a) for comparison. Also included are curves calculated from Figs. 8(a) and 8(b) for $h_c = 1.0$ and 1.5 ft. The experimental photographic points as measured are also included, and the scatter of these points from the calculated curve is seen to be small.

It is felt, then, that to within the reliability of the existing data the assumption made in drawing the locus $\ell - \ell$ of the triple point for various charge heights is valid as a working approximation.

II. PRESSURE RESULTS IN TERMS OF THE GEOMETRY OF THE REFLECTION PHENOMENON

5. Definition of variables used

The geometry of the reflection phenomenon discussed in the preceding section is used as a basis for the study of the pressure data obtained in the four bare-charge series and the three bomb series reported by UERL.[1,2] Again the data are reduced to the basis of 1 lb of TNT.

Two types of pressure-time records are encountered depending on the relative gauge, charge, and ground positions. If the gauge is above the triple-point height for the given charge height, two shocks will strike the gauge in succession, the incident shock I and the reflected shock R. The initial peak pressure, minimum pressure before second peak, and second or reflected peak pressure are defined as P_P, P_A, and P_R, respectively (corresponding to P, A, and R in Fig. 8 of Ref. 1). Since the reflected shock has traveled farther than the incident shock on arrival at the gauge and because of the time decay of the pressure behind the incident shock at the gauge before arrival of the reflected shock, it is convenient to define the following quantities for the pressures of the incident and reflected shocks in the reflection system. The pressure of the incident shock is taken as the peak pressure of the incident shock at the time the reflected shock arrives at the gauge. This pressure P_i is obtained from P_P by using reflection time data (Figs. 2 through 5), a velocity-pressure relation for shock waves in air,[9] and a pressure-distance exponent $n = 1.5$ in the expression $P = Ar^{-n}$. The pressure of the reflected shock is defined as $P_r = P_R - P_A + P_i$.

For gauges below the triple point, one shock is observed on the pressure-time records. This peak pressure is defined as P_M, corresponding to the pressure of the Mach shock or stem. The free-air pressure that would have been recorded at such a gauge in the absence of the ground is defined as P_F. This value was obtained from the pressure-distance law for 1 lb of TNT,[2] $P = 3.25(15.9/r)^{1.5}$. This law holds very well over the range of pressures studied.

The quantities necessary to compute α as defined in Fig. 1(b) for records from gauges above the triple point were obtained from Fig. 9(a) by

drawing an arc centered at the charge (that is, centered on the axis of ordinates at height h_c) with a radius equal to the distance from charge to gauge plus the distance traveled by the incident shock in the reflection time. The intersection of this arc with the proper curve of the family of Fig. 9(a) defines the point of reflection M of the shock system at the time the pressures of the incident and reflected shocks are compared. For gauges below the triple point, the simplifying assumption is made that the Mach stem is vertical so that α is the angle of incidence with the horizontal at a point directly above the gauge on the triple-point path. As in the preceding section, $\alpha_{extreme}$ is defined as a function of charge height.

For gauges above the triple point R_{gM} is defined as the distance, at the time of comparison of incident and reflected pressure, from M to the point on the reflected shock R at which the pressure was measured. A corresponding relative variable $(h_g - y)/y$ is defined for gauges below the triple point, where y is the height of stem. This is taken as zero when $h_g - y = 0$ even when y is zero, and it is taken as -1 if $h_g = 0$, $y \neq 0$, or if $y >> h_g$.

The variables chosen then to represent the pressure data are P_r/P_i, $\alpha - \alpha_{extreme}$, and R_{gM} for gauges above the triple point, and P_M/P_F, $\alpha - \alpha_{extreme}$, and $(h_g - y)/y$ for gauges below the triple point.

6. Summary of pressure data in terms of relative variables

In Figs. 12 through 26 the pressure ratios are plotted against the appropriate distance variables [R_{gM} for gauges above the triple point and $(h_g - y)/y$ for gauges below the triple point] for 15 ranges of $\alpha - \alpha_{extreme}$ and in each range a smooth curve has been drawn through the points. The appropriate value of P_r/P_i or P_M/P_F for a given value of the abscissa can be determined for any value of $\alpha - \alpha_{extreme}$ by linear interpolation between the value read from the curves in two successive ranges.

Included on these graphs are data from the four bare-charge series and three GP-bomb series carried out by UERL (Refs. 1 and 2) as well as data obtained at Princeton with $h_g = 0$ using $\frac{1}{2}$-lb TNT Engineer Blocks.[10] The value of P_F used for the Princeton data was taken from the pressure-distance curve reported in Ref. 10. No single-peak bomb records (gauges below triple point) are included in these figures.

It will be noted in these figures that there is no systematic trend with D. Although, for convenience, the data have not been plotted to show the effect of charge weight, again no significant systematic trend could be detected, and in this method of plotting, the effect of bomb case on the pressure ratios for records from gauges above the triple point was not apparent. "Best fitting" curves, smoothed by eye, were drawn through the data.

Figures 12 through 16 cover the range for $y = 0$, that is, regular reflection range and beginning Mach reflection range. In these figures, the very sharp rise at $R_{gM} = 0$ is to be noted. This indicates that the high overpressure due to oblique, regular reflection of shock waves is an extremely local phenomenon for spherical decaying shocks. Because of this sharp rise, the value of P_r/P_i at $R_{gM} = 0$, that is, at the triple point, is subject to considerable uncertainty. The smoothed curves, however, are felt to extrapolate to the correct value at $R_{gM} = 0$ to within about 10 percent. For $\alpha - \alpha_{extreme}$ in the range 10° to 16° (Fig. 17), the height of stem is very small at the values of D studied so that the values of $(h_g - y)/y$ from 0 to -1 (that is from $h_g = y$ to $h_g = 0$) cover a very small range of y(0 to $\ll 1$ ft). It was for this reason that the smoothed curve was drawn as shown.

Since for very low charge heights ($h_c < 2$ ft), the value of $\alpha - \alpha_{extreme}$ becomes very large ($\alpha \gg 90^\circ$), the data obtained for these charge heights are plotted in a different fashion. For these high values of $\alpha - \alpha_{extreme}$, the height of triple point is so great that the Mach shock has completely "swallowed up" the incident shock even at small values of D. Thus the dependence of the pressure ratio P_M/P_F on h_g is very small. It was possible, therefore, to plot P_M/P_F versus D from the available data for a series of constant charge heights of 0, 0.5, 1.0, 1.5, and 2.0 ft without regard to gauge height. These data are plotted in Fig. 27. The smoothed curves were drawn in a manner to fit the data which include results from 2-lb, 4-lb, 12-lb, and 40-lb bare charges, as well as to give a consistent family of curves.

7. Prediction of pressure versus charge height curve

It was felt that the most directly practical way of comparing these pressure data with the theory of regular reflection, as well as with the

results obtained by Smith with the Princeton shock tube, was to plot by the use of the curves of Figs. 12 through 27 the expected pressure versus charge height at a series of values of $\underline{D}$ and h_g.

Necessary for these pressure versus charge height curves are the free-air pressures to be expected at a given distance from the charge. As discussed previously, the law $P = 3.25(15.9/r)^{1.5}$ for 1 lb of TNT holds well over the range from about 1 lb/in^2 to about 6 lb/in^2. However, it was felt desirable to attempt to predict the pressure distribution for D = 7 ft, h_g = 0, 2, and 4 ft. For these curves, some further free-air pressure data are required. A point at r = 5.85 ft, P = 21.5 lb/in^2 was obtained in a recent explosive comparison series on 41.7-lb bare charge.[11] The final pressure-distance law used, then, is plotted on log-log paper in Fig. 28.

Also necessary for obtaining the value of P_r (second peak) for the larger values of h_c (those that give a double-peak record for a given gauge position) are data giving the reflection time as a function of gauge position from a given charge position and the time-decay constant of a shock as a function of peak pressure.

Figure 29 is a series of curves giving reflection time as a function of $\underline{D}$ for various values of charge height and gauge height. These curves were drawn from data at 10.4 ft (Fig. 2), 15.9 ft (Figs. 3 and 4), and 39.8 ft (Fig. 5). The triple-point paths [Figs. 9($\underline{a}$) and 9($\underline{c}$)] predicted from the reflection time data at 10.4 ft and 15.9 ft were used to give the value of $\underline{D}$ for a given charge height and gauge height at which the reflection time is zero. The curves of Fig. 29 are felt to be reliable to within 10 percent or less except possibly for the larger values of h_g and h_c at D < 10 ft.

The time-decay constant of the shock for bare charges of TNT, defined linearly in the form $\tau = (P_P - P_A)/\text{Reflection time}$, was computed for most of the records studied. Figure 30 is a family of straight lines (on log-log paper) each member of which relates $\underline{\tau}$ with the peak pressure of the shock for a small range of values of reflection time. The experimental points were, for convenience, not included in this figure. However, the average deviation of all measured values of $\underline{\tau}$ from those calculated by linear

interpolation among the family of Fig. 30 is approximately 17 percent. The data from which Fig. 30 was drawn include pressures in the range 1 to 21 lb/in.^{2} with the majority of the data in the range 1 to 6 lb/in.^{2}

By use, then, of Figs. 12 through 26 and Figs. 27 through 30, it is possible to compute data for curves of pressure versus charge height for various values of h_g at any value of $\underline{D}$ from approximately 7 ft to approximately 40 ft. Extrapolation of the actual experimental data is, of course, involved in calculations for $D < 10$ ft. Extrapolation is also involved for $h_g < 1$ ft except for $D = 15.9$ ft.[2] Figures 31 through 35, then, give the pressure distribution versus charge height for various values of gauge height and horizontal distance from charge. Included in these figures are the incident Mach pressures, P_M, for the lower values of h_c which give single-peak records, as well as P_P and P_R, incident and reflected peak pressures, for the higher values of h_c which give double-peak records.

Also included on the curves for $h_g = 0$ in Figs. 31 through 34 are data reported by Taub[10] computed from the theory of regular reflection as well as from the Princeton shock-tube results. These data are based on the pressure-distance curve plotted in Ref. 10. The quantity P_M plotted in these figures is the pressure on a single-peak record which could mean one of two things:

1. $h_g = 0, \quad y \geqq 0$
2. $h_g > 0, \quad y \geqq h_g.$

Examples of the use of Figs. 12 through 30 for the construction of Figs. 31 through 35 are given in the following.

Example 1. -- As an example of the calculation of P_R and P_P for a double-peak record, the values $h_g = 2.0$ ft, $D = 20$ ft, and $h_c = 6.0$ ft will be taken (Fig. 34). From Fig. 29, the reflection time is found to be 0.65 msec.

A value of $\underline{r}$ from charge to gauge of 20.35 ft (calculated from the assumed values of $\underline{h}_g$, $\underline{D}$, and h_c) leads by Fig. 28 to a value of P_P of 2.24 lb/in.^{2} for 1 lb of TNT.

A value for $\underline{c}$ of 1.20 ft/msec was taken as the average velocity of the incident shock.[9] In the reflection time 0.65 msec, therefore, the incident shock traveled a distance of $1.20 \times 0.65 = 0.78$ ft. Thus the radius of the incident shock at the time the reflected shock arrived at the gauge was

20.35 + 0.78 = 21.13 ft. With this value for the radius of the incident shock, Fig. 28 gives a value of $P_i = 2.14$ lb/in^2.

Next, on Fig. 9(a), describe an arc of radius 21.13 ft centered at $h_c = 6$ ft, D = 0 ft (that is, centered on the axis of ordinates at the height 6 ft). This arc intersects the $\ell - \ell$ locus for a value of $h_c = 6$ ft (the curve with the number 6 adjacent to it) at a value of y = 0.95 ft, D = 20.60 ft. The value of R_{gM}, the distance from this latter point to y = 2 ft, D = 20 ft (the gauge position), is calculated to be 1.20 ft. Now

$$\alpha = \tan^{-1} \frac{D}{h_c - y} = \tan^{-1} \frac{20.60}{6.0 - 0.95} = 77.4^\circ.$$

By Fig. 7 $\alpha_{extreme}$ for $h_c = 6$ ft is 46.2°. Thus $\alpha - \alpha_{extreme} = 31.2^\circ$.

Linear interpolation between Fig. 20 ($\alpha - \alpha_{extreme} = 28^\circ$ to 34°, hence center of range is 31°) and Fig. 21 (center of range, 37°) at $R_{gM} = 1.20$ ft leads to a value of $P_r/P_i = 1.66$. Therefore

$$P_r = P_i + P_R - P_A = 1.66 \times P_i = 1.66 \times 2.14 = 3.55 \text{ lb/in}^2$$

Thus

$$P_R - P_A = 3.55 - P_i = 1.41 \text{ lb/in}^2$$

In order to obtain P_R a value of P_A is necessary. For this a value of $\underline{\tau}$ of 1.01 (lb/in^2)/msec is obtained from Fig. 30 by use of the proper value of the reflection time (0.65 msec) at the proper value of P_P (2.24 lb/in^2). Since by definition

$$\tau = (P_P - P_A)/\text{Reflection time},$$

$$1.01 = (2.24 - P_A)/0.65,$$

$$P_A = 1.58 \text{ lb/in}^2$$

Thus

$$P_R = 1.41 + 1.58 = 2.99 \text{ lb/in}^2$$

This value of P_R and the value $P_P = 2.24$ lb/in^2 are the points plotted in Fig. 34 for $h_g = 2.0$ ft, D = 20 ft, and $h_c = 6$ ft.

Example 2. -- As an example of the calculation of P_M for a single-peak record, the values $h_g = 0.0$ ft, D = 20 ft, $h_c = 6.0$ ft will be taken (Fig. 34). Here, of course, the reflection time is zero.

The value of $\underline{r}$ for these assumed conditions is 20.85 ft and from Fig. 28 it is found that $P_F = 2.15$ lb/in^2

On the assumption that the stem is vertical, the point of reflection is on the $\ell - \ell$ locus for $h_c = 6.0$ ft at a value of $D = 20.0$ ft which by Fig. 9(a) leads to the value $y = 0.85$ ft.

The angle α is calculated as in Example 1, and is found to be 75.6°. Using the same value 46.2° for $\alpha_{extreme}$ (the value of h_c is the same) as in Example 1, $\alpha - \alpha_{extreme} = 29.4^\circ$.

Since $h_g = 0$, $(h_g - y)/y = -1$ and in accordance with the definition of this variable $y \neq 0$. By interpolating between Figs. 19 and 20 at $(h_g - y)/y = -1$, the value of P_M/P_F is found to be 2.22; and $P_M = 2.22 \times 2.15 = 4.78$ lb/in^2.

In cases of single-peak records for which $\alpha - \alpha_{extreme}$ is greater than about 75° (the limit of Fig. 26), use is made of Fig. 27 wherein P_M/P_F is plotted against D for values of charge height less than 2 ft. The curves of Figs. 12 through 26 plus the curves of Fig. 27 (in combination with other curves of this report) give the data required for calculating peak pressures for most configurations of h_c, h_g, and D.

It must be kept in mind that the pressure-distance curve of Fig. 28, the time-decay constant curves of Fig. 30, and thus the pressure versus charge height curves of Figs. 31 through 35 are valid only for bare charges. However, an approximate percentage correction for the effect on pressure of the case of a given bomb could be applied to the scaling factor $W^{1/3}$ used in converting to the net charge weight W.

The curves of Figs. 32, 33, and 35 for $h_g > 0$ are in essential agreement with corresponding curves reported in Refs. 1 and 2. This, of course, only shows that this method of representing the data has not altered the original data on which it is based. The agreement with the data reported in Ref. 10 for $h_g = 0$ is seen to be satisfactory. Probably the poorest agreement between the predicted pressure versus charge height curves and the data reported in Ref. 10 calculated from regular reflection theory and the Princeton shock-tube results based on the free-air pressure-distance curve reported in Ref. 10 is in Fig. 33 for $h_g = 0$, $D = 15$ ft. This refers to both the pressure level, when account is taken of the difference between the free-air pressure-distance curve reported in Ref. 10 and that given in Fig. 28, and to the position of the maximum pressure. The UERL data are most

complete at approximately this value of D for low gauge heights.[2] No comparison with independent data is possible for some of the curves calculated. It is felt that until further experimental data are available this method of predicting pressure distributions is useful.

It might be mentioned that satisfactory comparisons of some of the data reported here have been made with recent British work.[13]

III. OPTIMUM CHARGE HEIGHT FOR PEAK PRESSURE AND IMPULSE

A comparison has been made of the charge height which maximizes the pressure or impulse at a given gauge height and distance (a given h_g and D) with that which gives a height of stem equal to h_g for the given value of D. By use of these comparisons and the curves of Fig. 9(a), a prediction can be made of the height of charge required to maximize the pressure or impulse at a given point in space. It is felt that extrapolation of these data to points in space not studied experimentally can be carried out, at least for the pressure maximum.

8. Optimum charge height for pressure

In Fig. 36(a), the ratio of the charge height to produce a pressure maximum ($h_{c,opt}$) to that which produces a triple point ($h_{c,y}$) at the gauge has been plotted against gauge height. These data are averaged over D. Included are optimum charge heights taken from the experimental pressure versus charge height curves published in Refs. 1 and 2, as well as optimum charge heights taken from the predicted pressure versus charge height curves (Figs. 31 through 35). It will be noted that within the measurement scatter, this ratio $h_{c,opt}/h_{c,y} = 0.9$ is independent of gauge height.

In Fig. 36(b), the same ratio is plotted against D averaged over h_g. The same data are included. No dependence on D can be noted. Thus, in order to find the charge height required to maximize the pressure at a given point in space it is only necessary to find [by interpolation in Fig. 9(a)] the charge height which produces a height of stem equal to h_g at the given value of D and multiply this value by 0.9.

9. Optimum charge height for impulse

In Fig. 37(a), the ratio of the charge height to produce an impulse maximum ($h_{c,opt}$) to that which produces a triple point ($h_{c,y}$) at the gauge has been plotted against D. Here the data have been averaged over $h_g (h_g > 0.80)$ since no trend was detected with gauge height in this range of gauge heights. However, the scatter is considerably greater than in the case of the pressure maximum because the I, h_c-curves are much flatter than the P, h_c-curves. The

optimum charge heights for impulse were taken from the experimental impulse versus charge height curves published in Ref. 1.

In Fig. 37(b), the same ratio for impulse for low gauge heights has been plotted against h_g at D = ~15.9 ft, the only value of D for which data were available in this range of gauge heights.[2] In this range, a considerable trend with gauge height can be noted.

It is felt that Fig. 37(a) used in conjunction with Fig. 9(a) may be used to predict optimum charge heights for impulse to within the precision of the location of the maximum of the impulse versus charge height curves of Ref. 1, as long as the point at which the impulse is to be maximized has a reduced height from the ground of greater than 0.8 ft. For lower gauge heights than this, the data of Fig. 37(b) at D = 15.9 ft could give an indication of the correction to be applied to Fig. 37(a) for some other value of D.

References

1. "The effect of air-burst on the blast from bombs and small charges, I. Experimental results," by W. D. Kennedy, OSRD-4246, Sept. 1944.

2. "The effect of height of detonation on peak pressure and positive impulse measured close to the ground," by W. D. Kennedy and R. F. Arentzen, included in AES-5 (OSRD-4514), Dec. 1944.

3. "Oblique reflection of shocks," by John von Neumann, Bureau of Ordnance, Explosives Research Report No. 12, October 12, 1943.

4. "Analysis of data on shock intersections," Progress Report I, by P. C. Keenan and R. J. Seeger, Bureau of Ordnance, Explosives Research Report No. 15, February 3, 1944.

5. "Spark photographs of the Mach effect," by Col. Paul Liebessart, R.C. 417, May 1944.

6. "Regular reflection of shocks in ideal gases," by H. Polachek and R. J. Seeger, Bureau of Ordnance, Explosives Research Report No. 13, February 12, 1944.

7. "Mach reflection of shock waves from charges detonated in air," by R. G. Stoner, included in AES-3 (OSRD-4257), Oct. 1944.

8. "The reflection of shock waves in air," by L. G. Smith, included in AES-1 (OSRD-4076), Aug. 1944.

9. Final Report on "The hydrodynamic theory of detonation and shock waves," to June 30, 1941, by G. B. Kistiakowsky and E. Bright Wilson, Jr., OSRD-114, June 1941.

10. "Peak pressure dependence on height of detonation," by A. H. Taub, included in AES-1 (OSRD-4076), Aug. 1944.

11. "Order of effectiveness of explosives, III," by W. D. Kennedy, included in AES-4 (OSRD-4356), Nov. 1944.

12. "Order of effectiveness of explosives, IV. Peak pressures and positive impulses in the blast from 500-lb GP bombs filled with HBX, Torpex 2, Composition B, and Tritonal," by W. D. Kennedy, R. F. Arentzen, and C. W. Tait, included in AES-6 (OSRD-4649), Jan. 1945.

13. "The effect of height of burst on the blast characteristics from 67 lb bare charges of RDX/TNT 60/40," Armament Research Department, Interim Report, Dec. 1944. (WA-3502-6b).

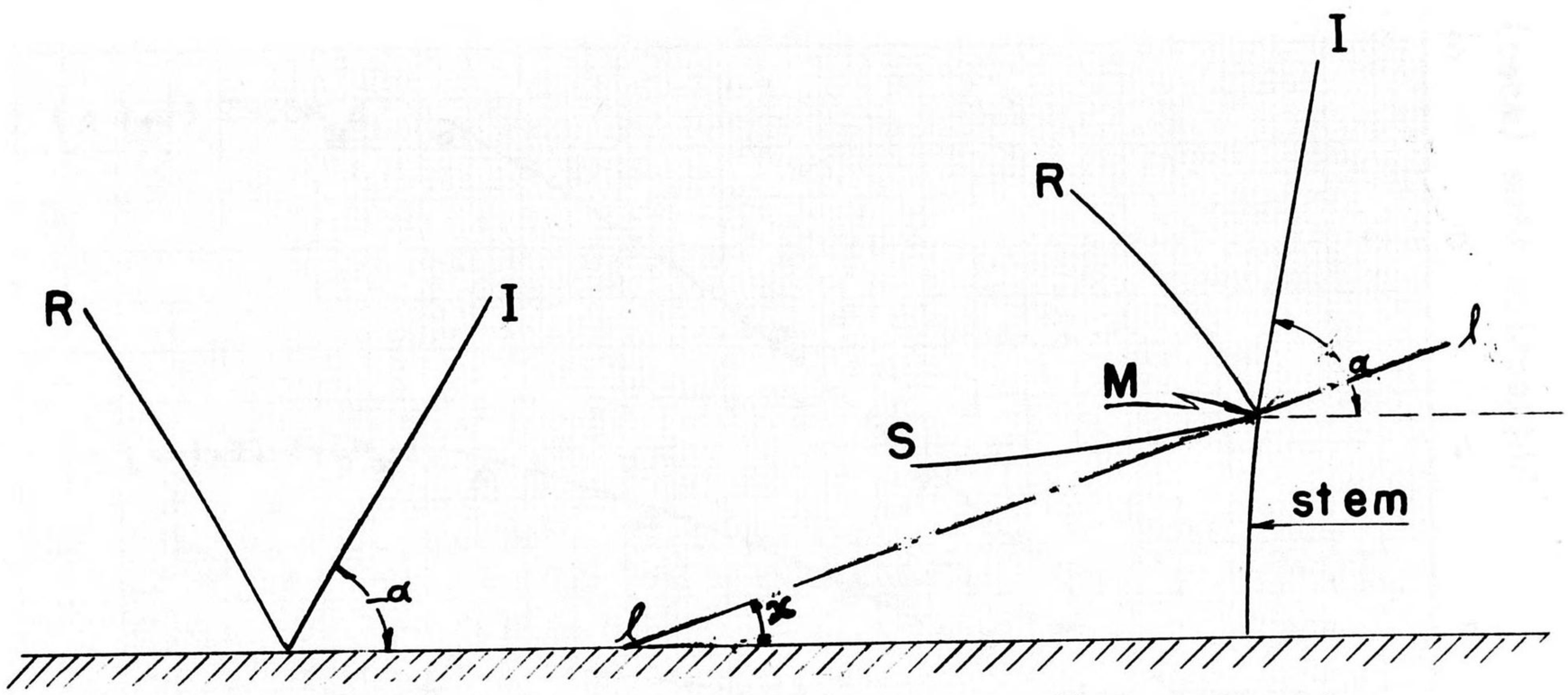

(a) Plane step shock.

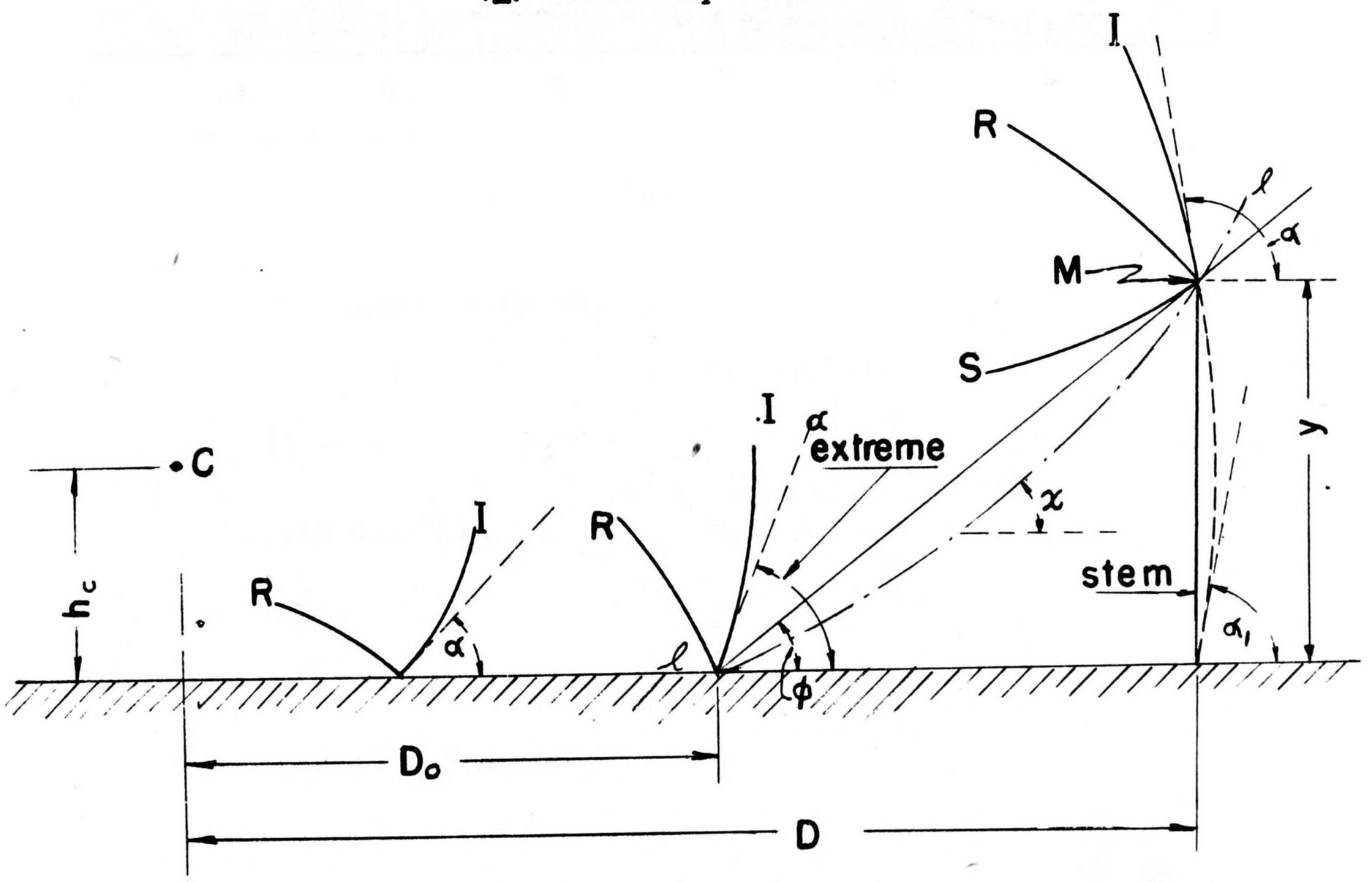

(b) Spherical shock.

Fig. 1. Regular and Mach reflections.

D = 10.4 ft

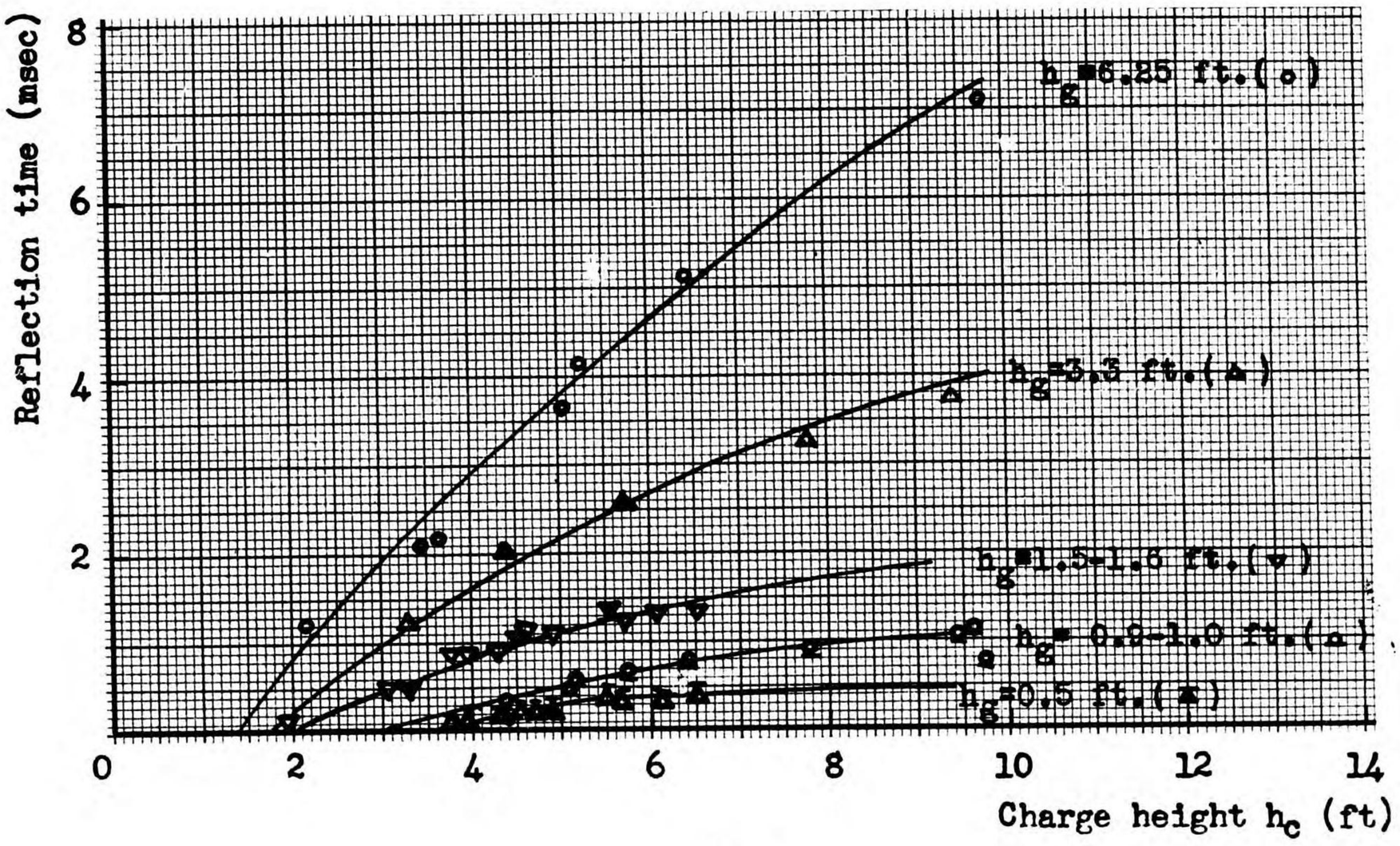

(a)

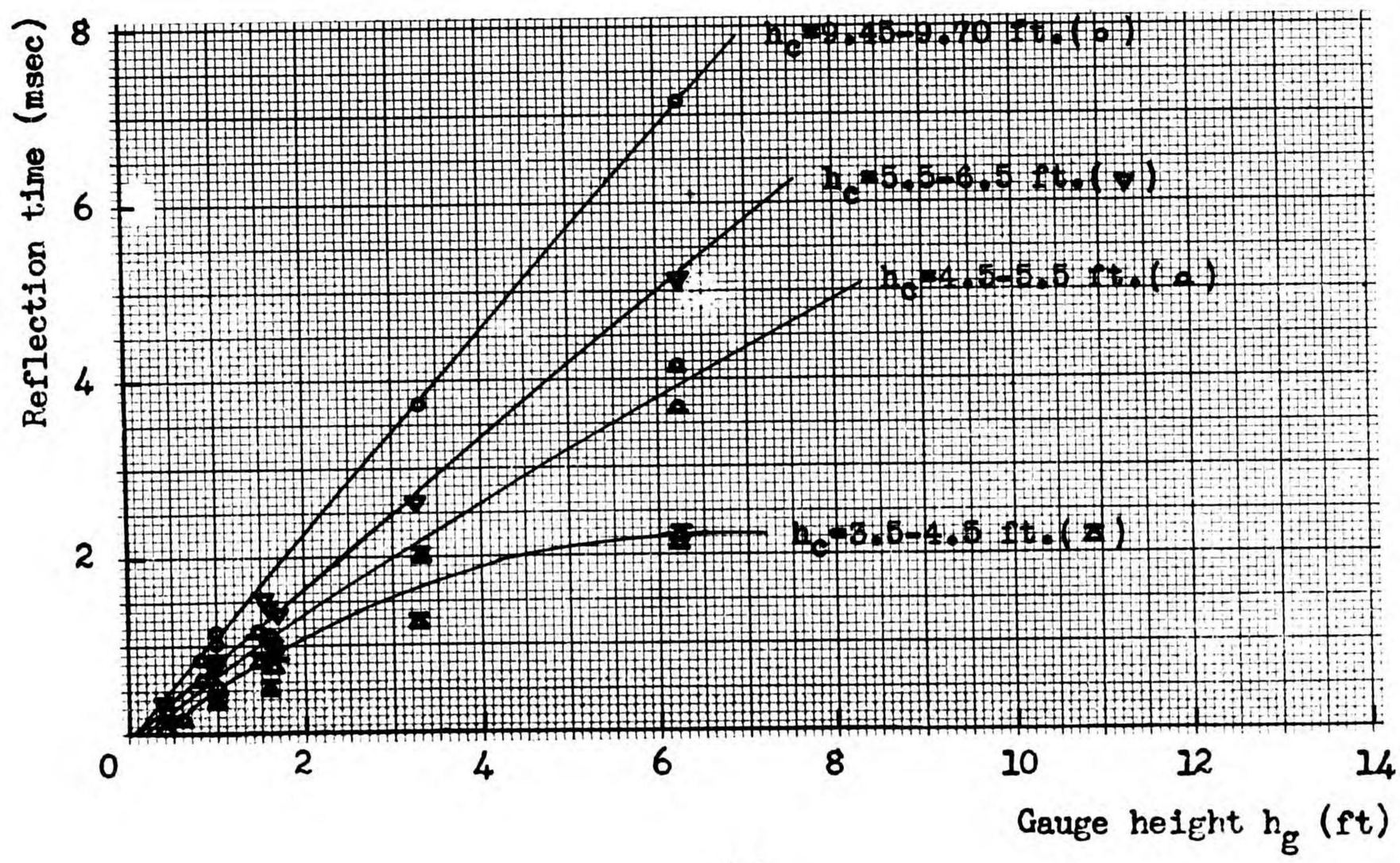

(b)

Fig. 2. Reflection time (a) versus charge height at constant gauge height, (b) versus gauge height at constant charge height.
All units reduced to basis of 1 lb TNT.

D = 15.9 ft

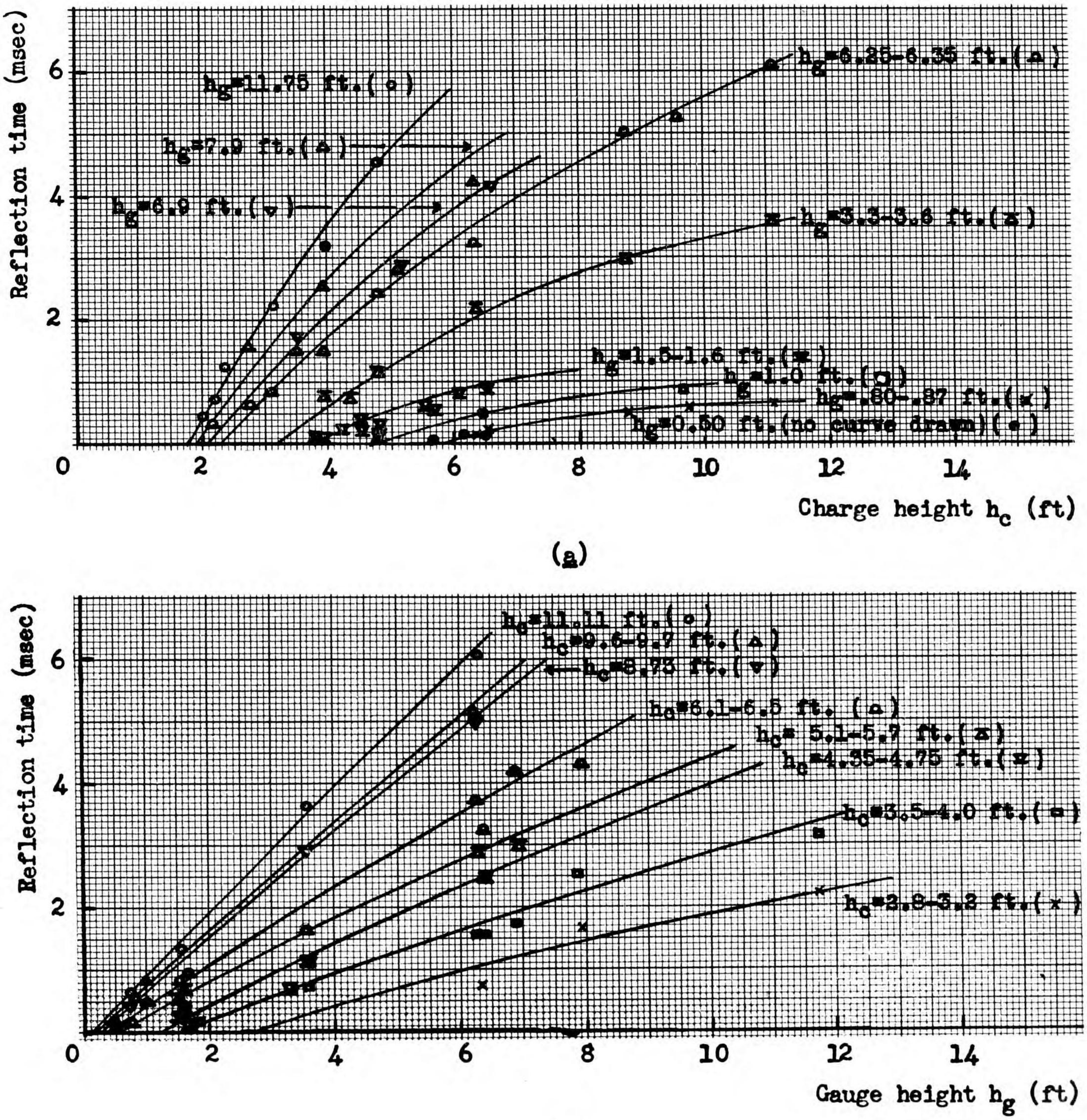

(a)

(b)

Fig. 3. Reflection time (a) versus charge height at constant gauge height, (b) versus gauge height at constant charge height.
All units reduced to basis of 1 lb TNT.

D = 15.7 ft

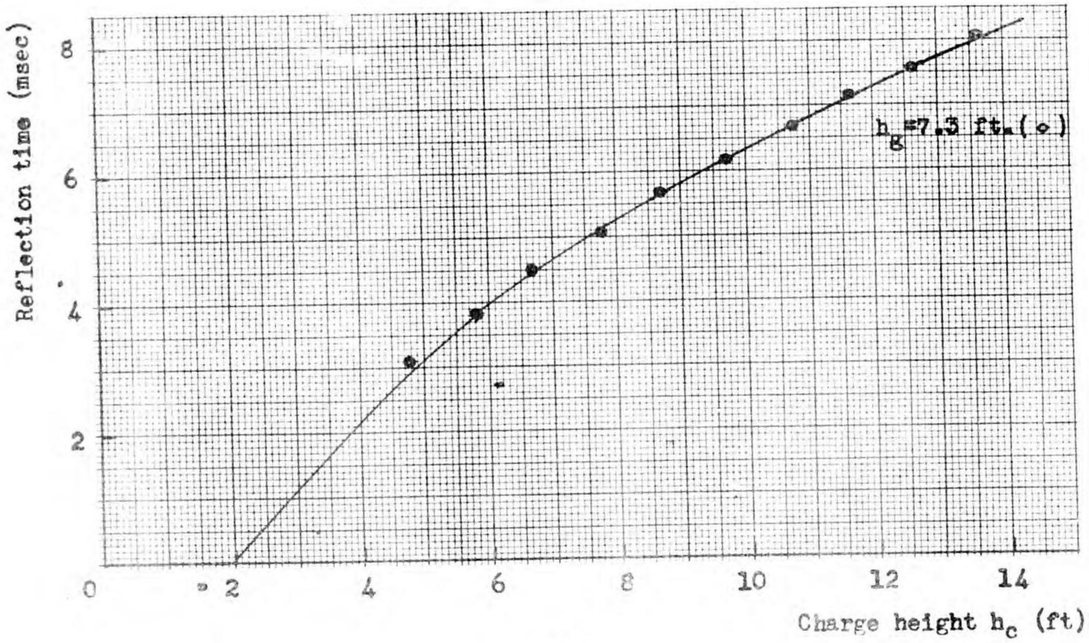

(a)

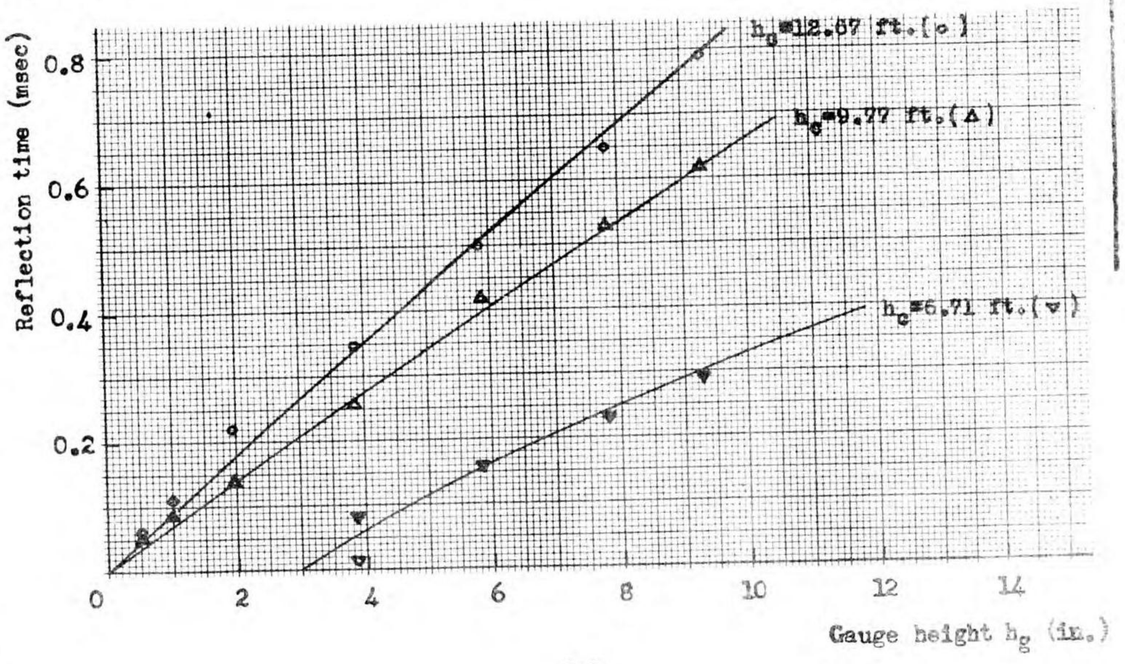

(c)

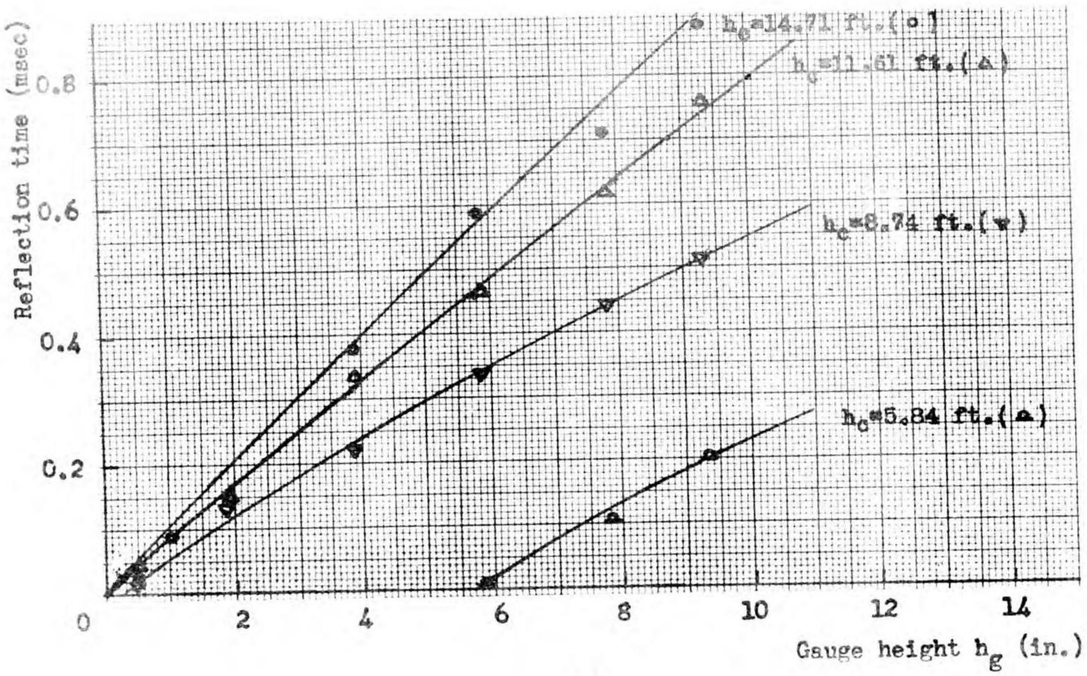

(b)

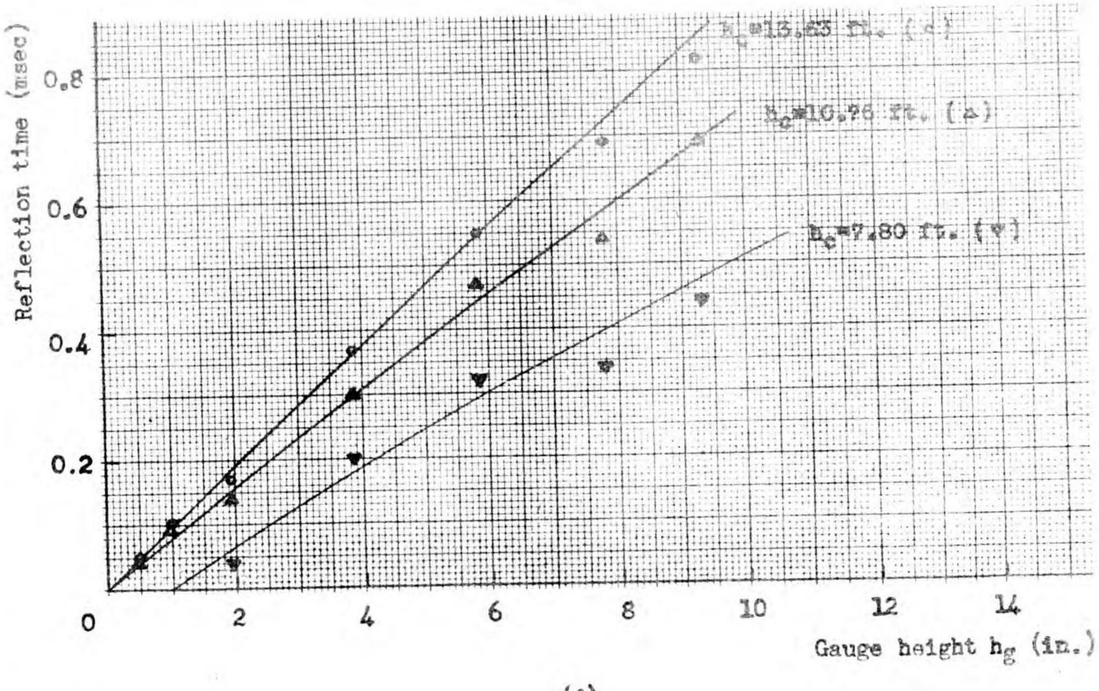

(d)

Fig. 4. Reflection time (a) versus charge height at constant gauge height; (b), (c), (d) versus gauge height at constant charge height.
All units reduced to basis of 1 lb TNT.

D = 39.8 ft

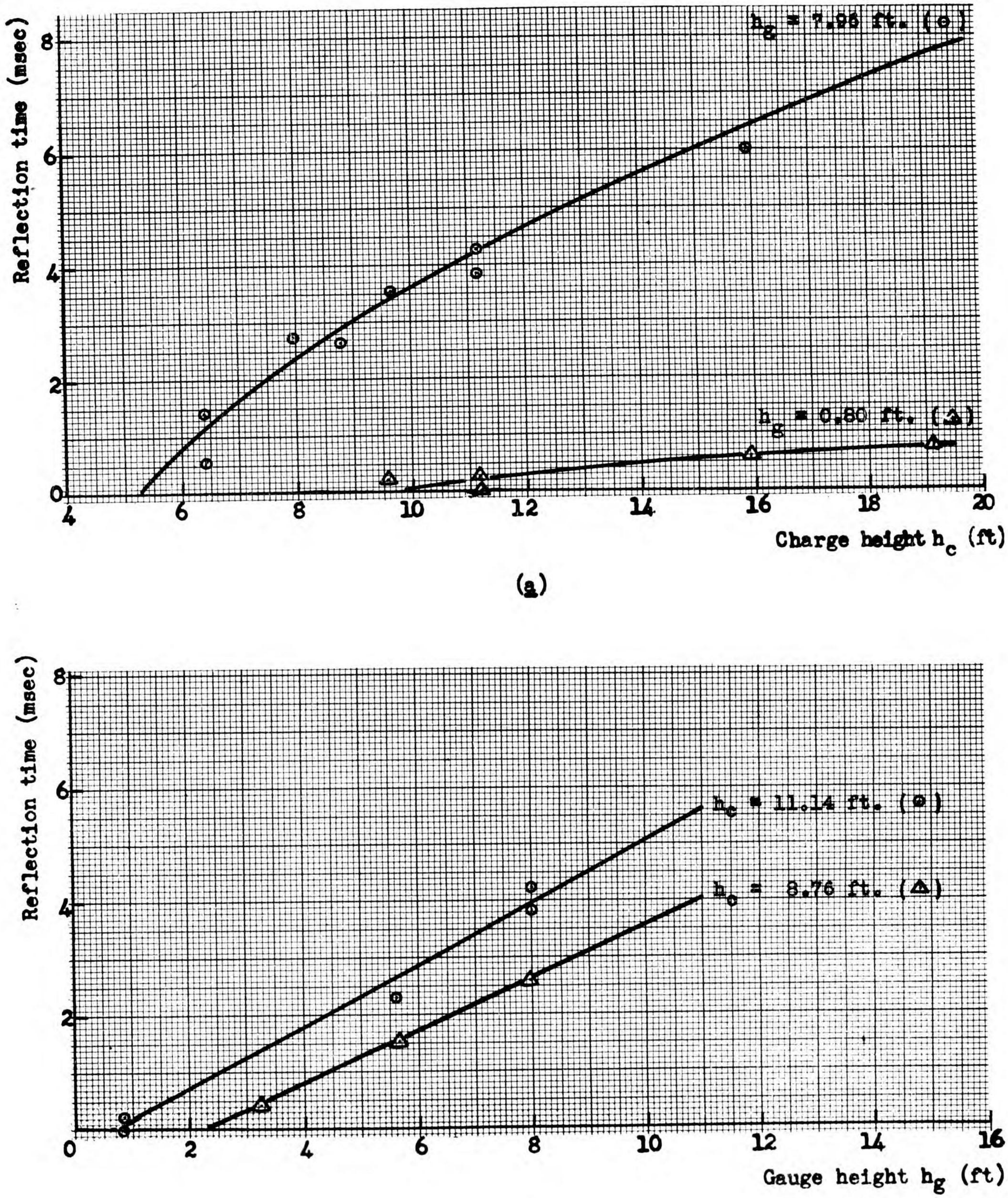

(a)

(b)

Fig. 5. Reflection time (a) versus charge height at constant gauge height, (b) versus gauge height at constant charge height.
All units reduced to basis of 1 lb TNT.

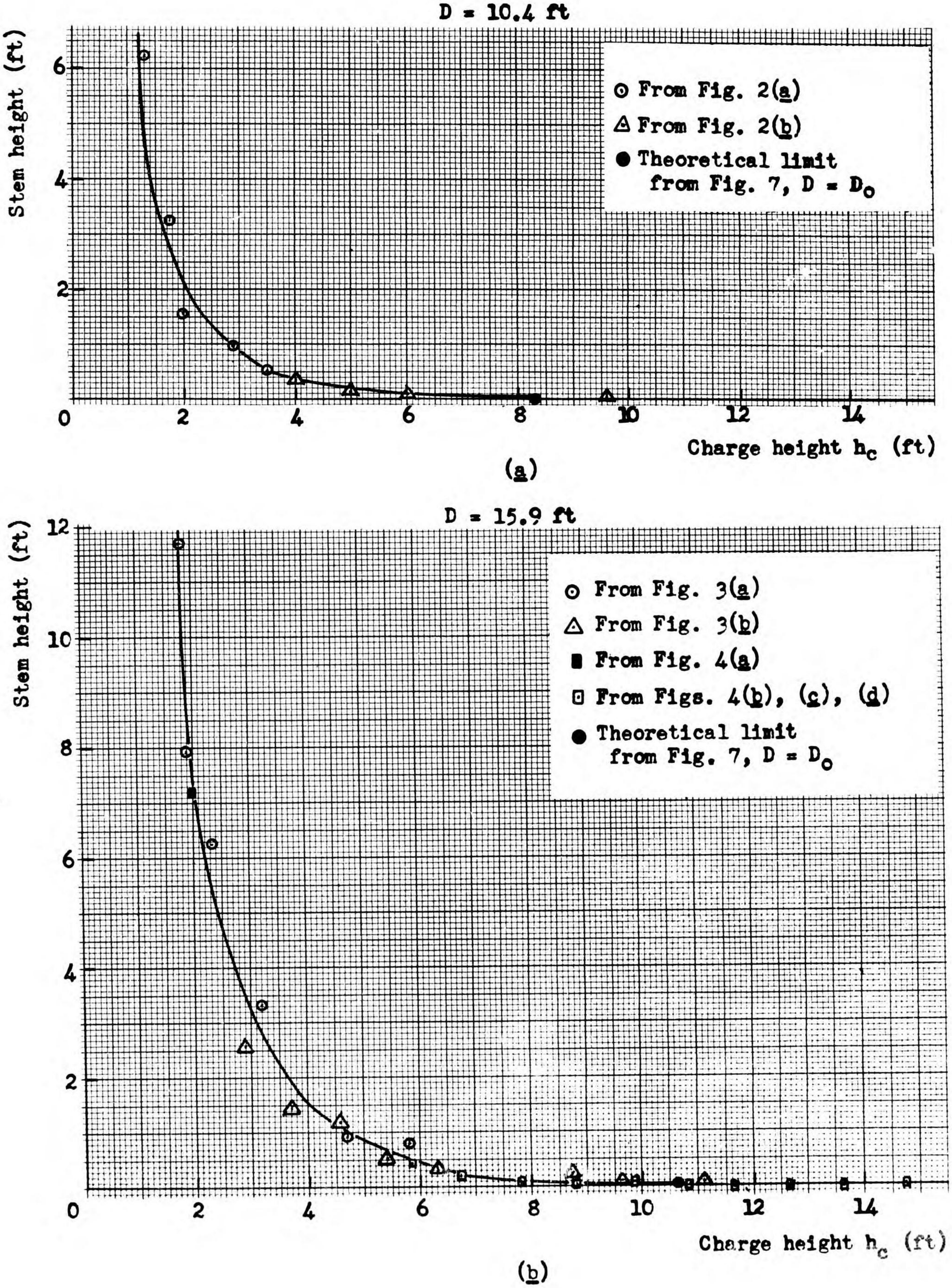

Fig. 6. Height of stem versus height of charge: (a) D = 10.4 ft; (b) D = 15.9 ft. All units reduced to basis of 1 lb TNT.

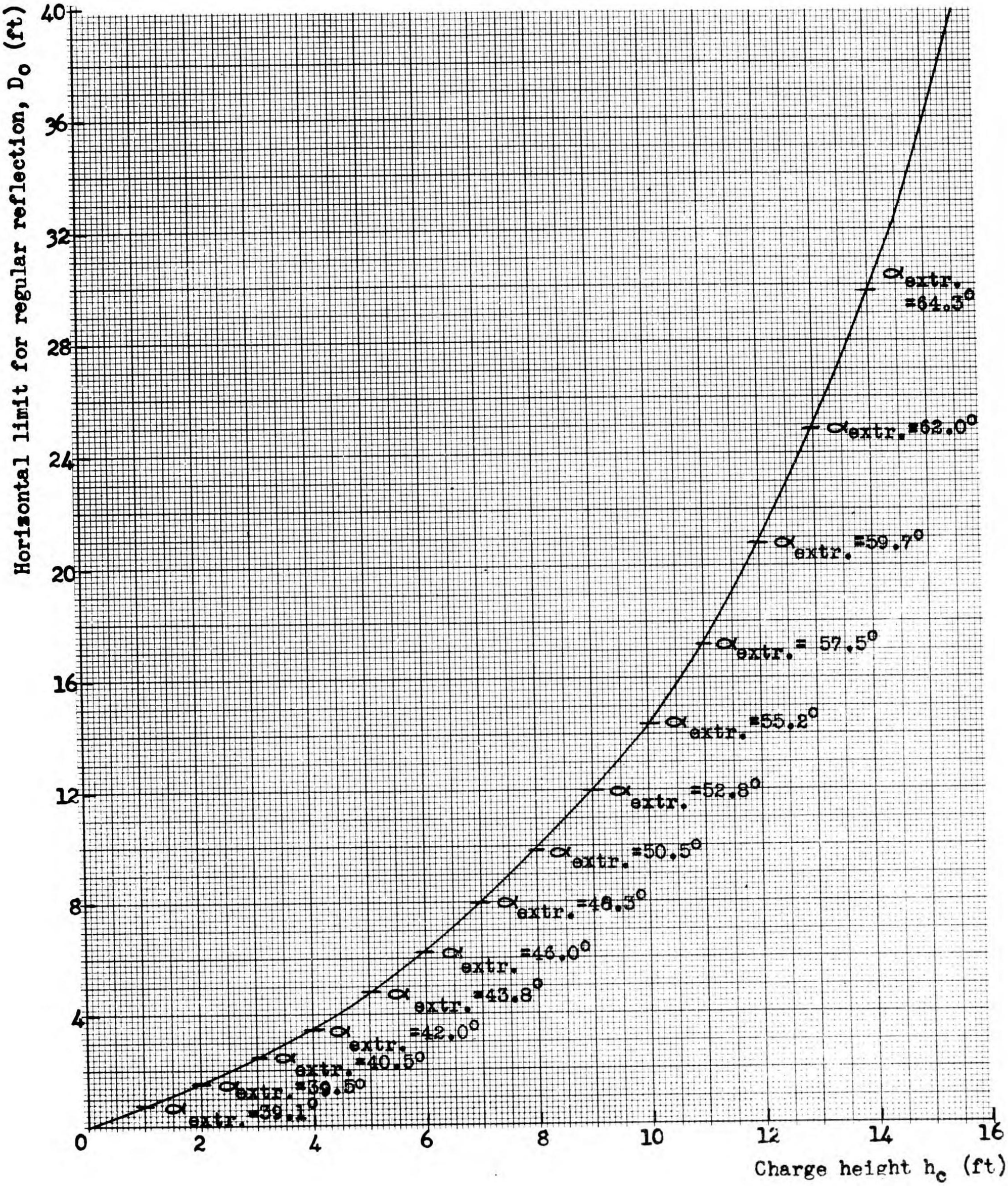

Fig. 7. Theoretical limits for regular reflection versus charge height. All units reduced to basis of 1 lb TNT.

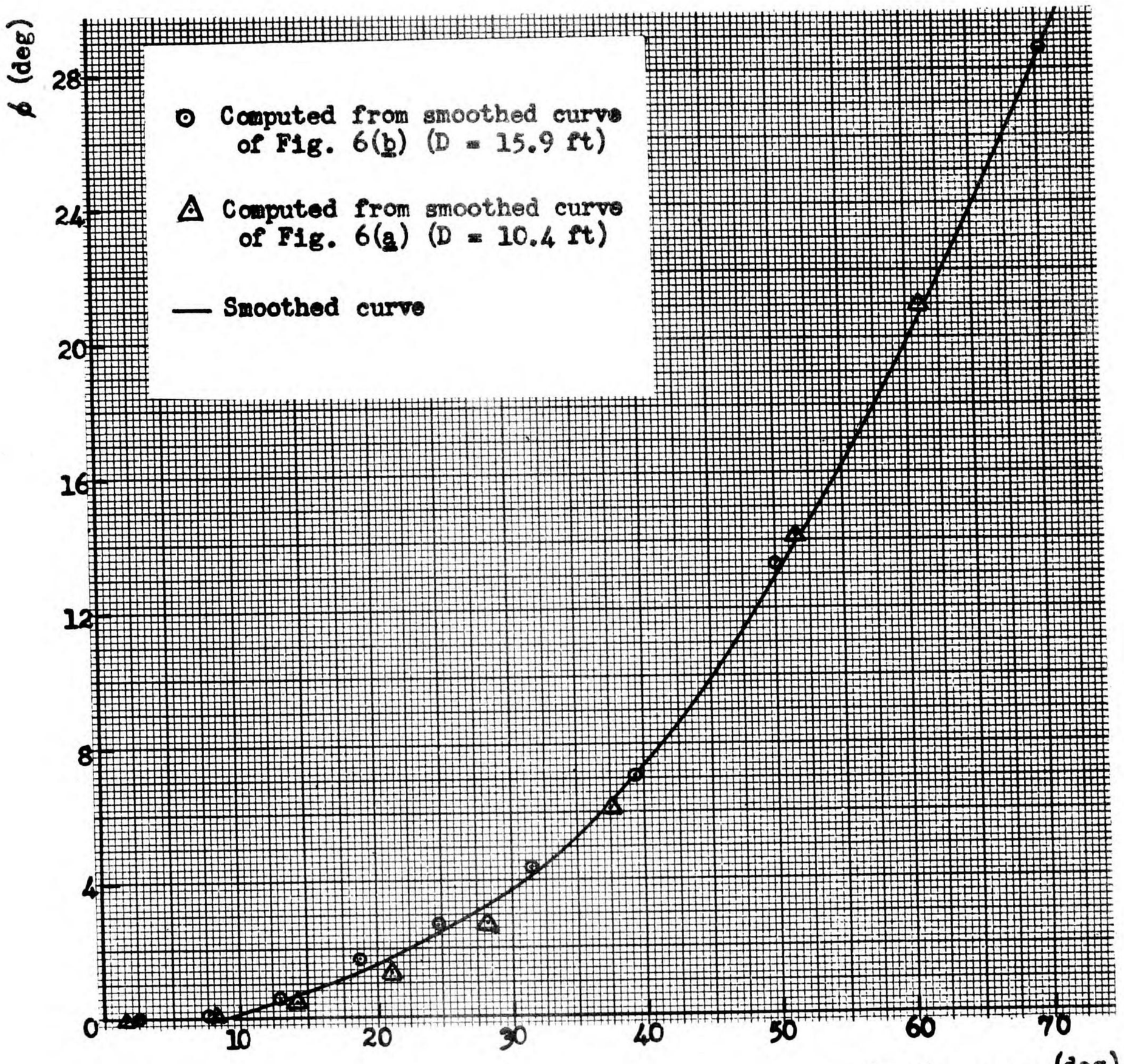

Fig. 8(a). ϕ versus $\alpha - \alpha_{extreme}$.
All units reduced to basis of 1 lb TNT.

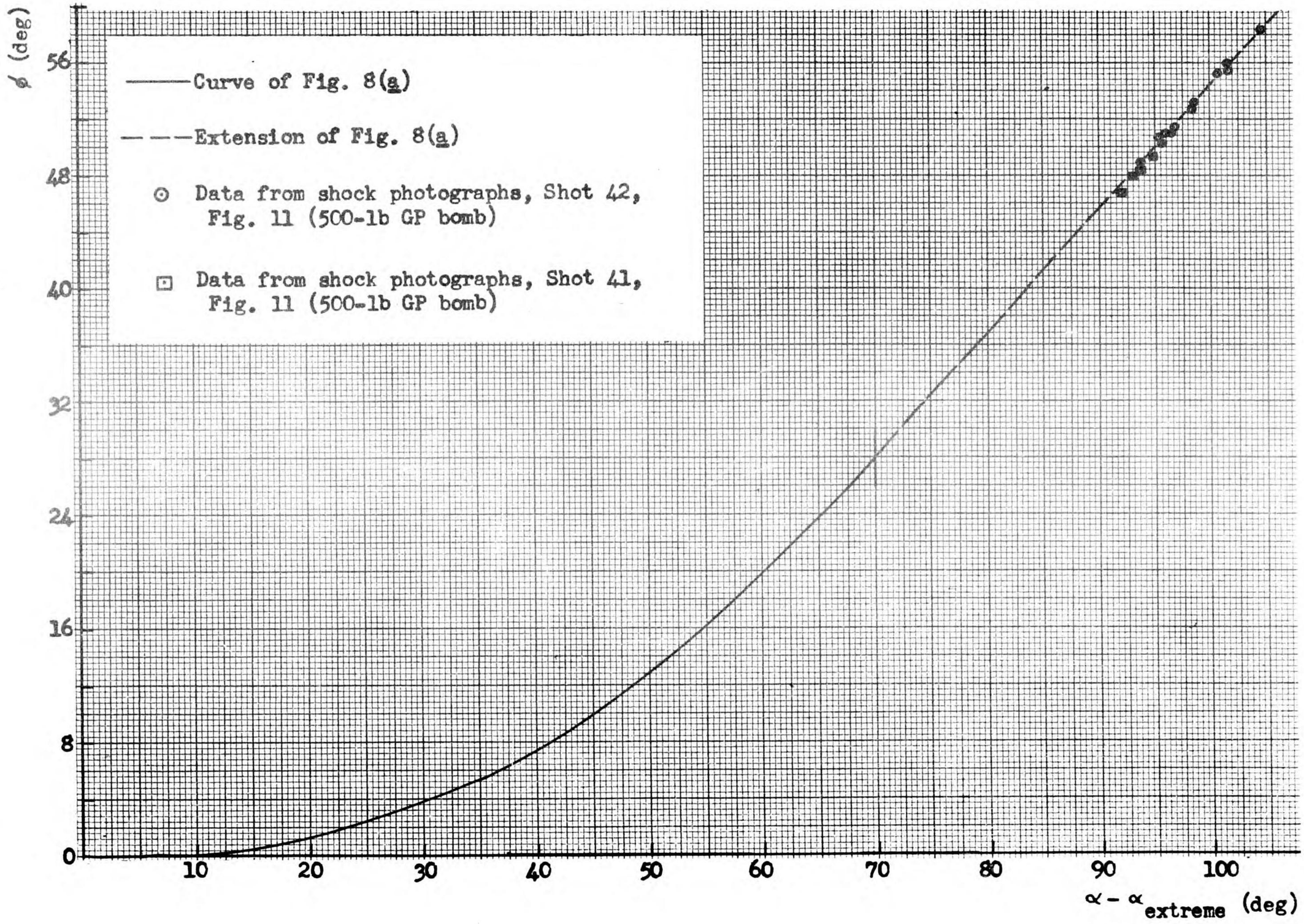

Fig. 8(b). ϕ versus $\alpha - \alpha_{extreme}$, including data from high-speed motion pictures.

CONFIDENTIAL

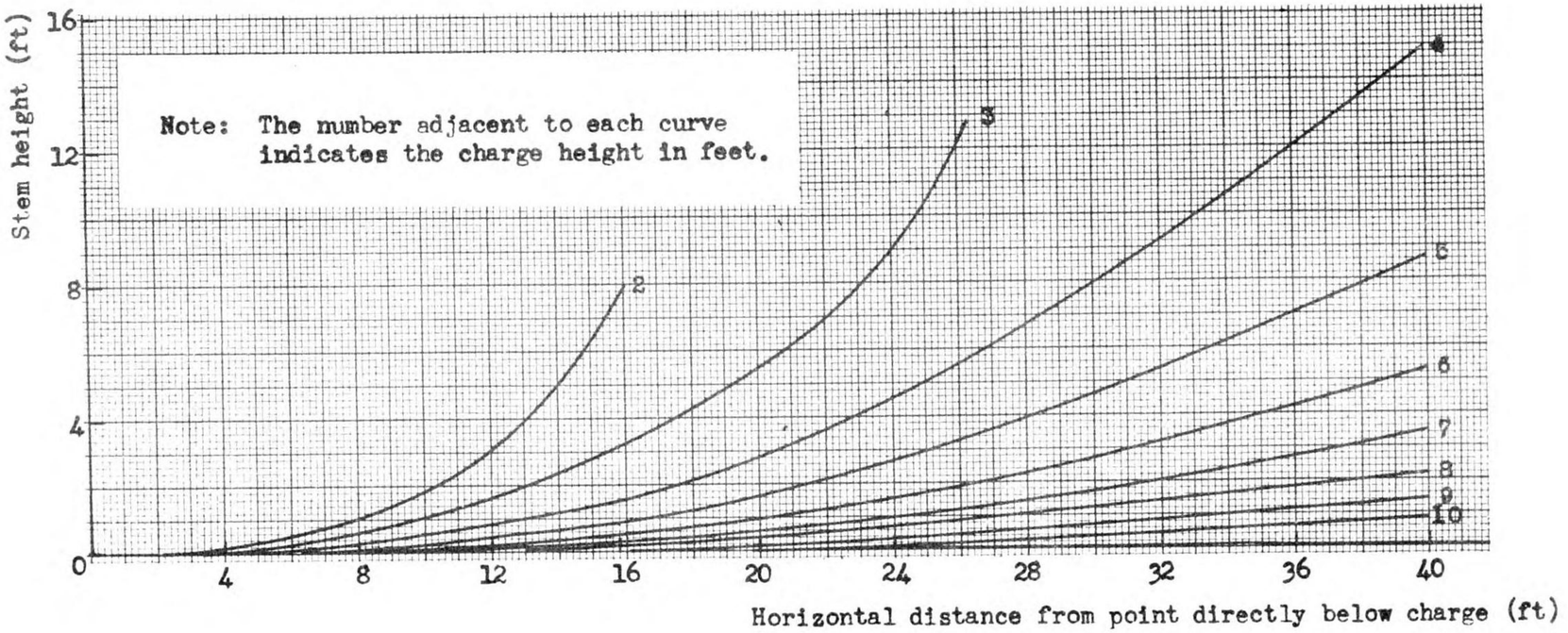

(a)

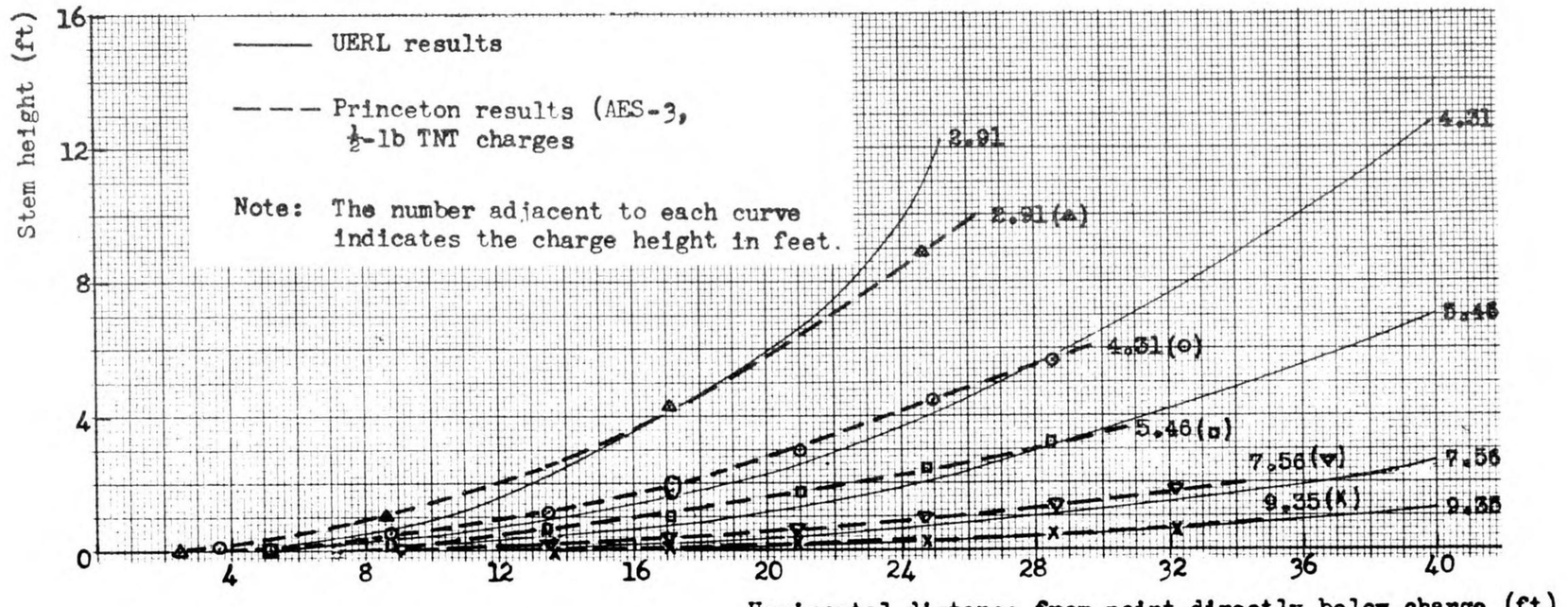

(b)

Fig. 9(a) and (b). Height of stem versus horizontal distance for various charge heights: (a) calculated values; (b) experimental values from Princeton and from Underwater Explosives Research Laboratory. All units reduced to basis of 1 lb TNT.

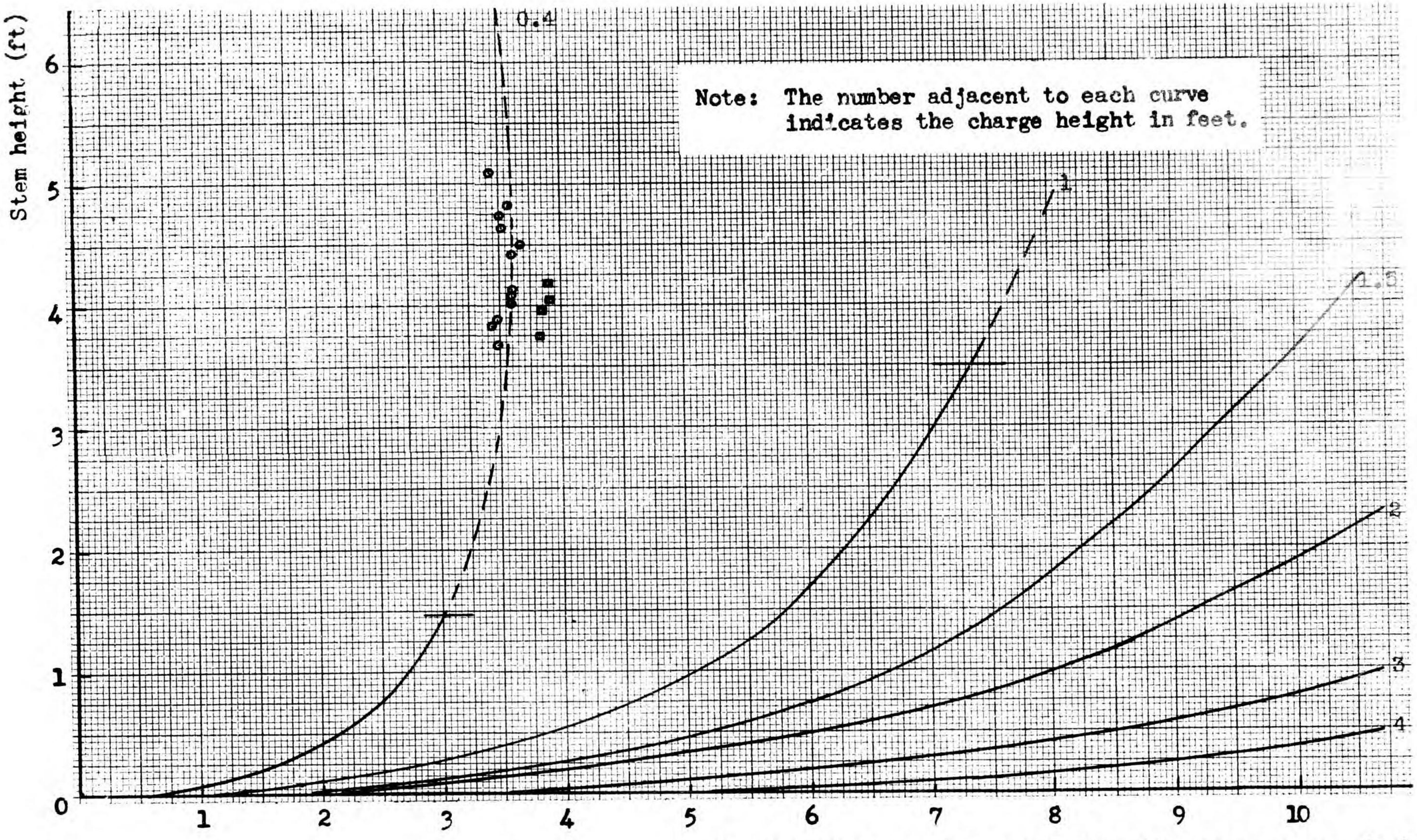

Fig. 9(c). Height of stem versus horizontal distance for various charge heights, including data from high-speed motion pictures.

All units reduced to basis of 1 lb TNT.

CONFIDENTIAL

D = 39.8 ft

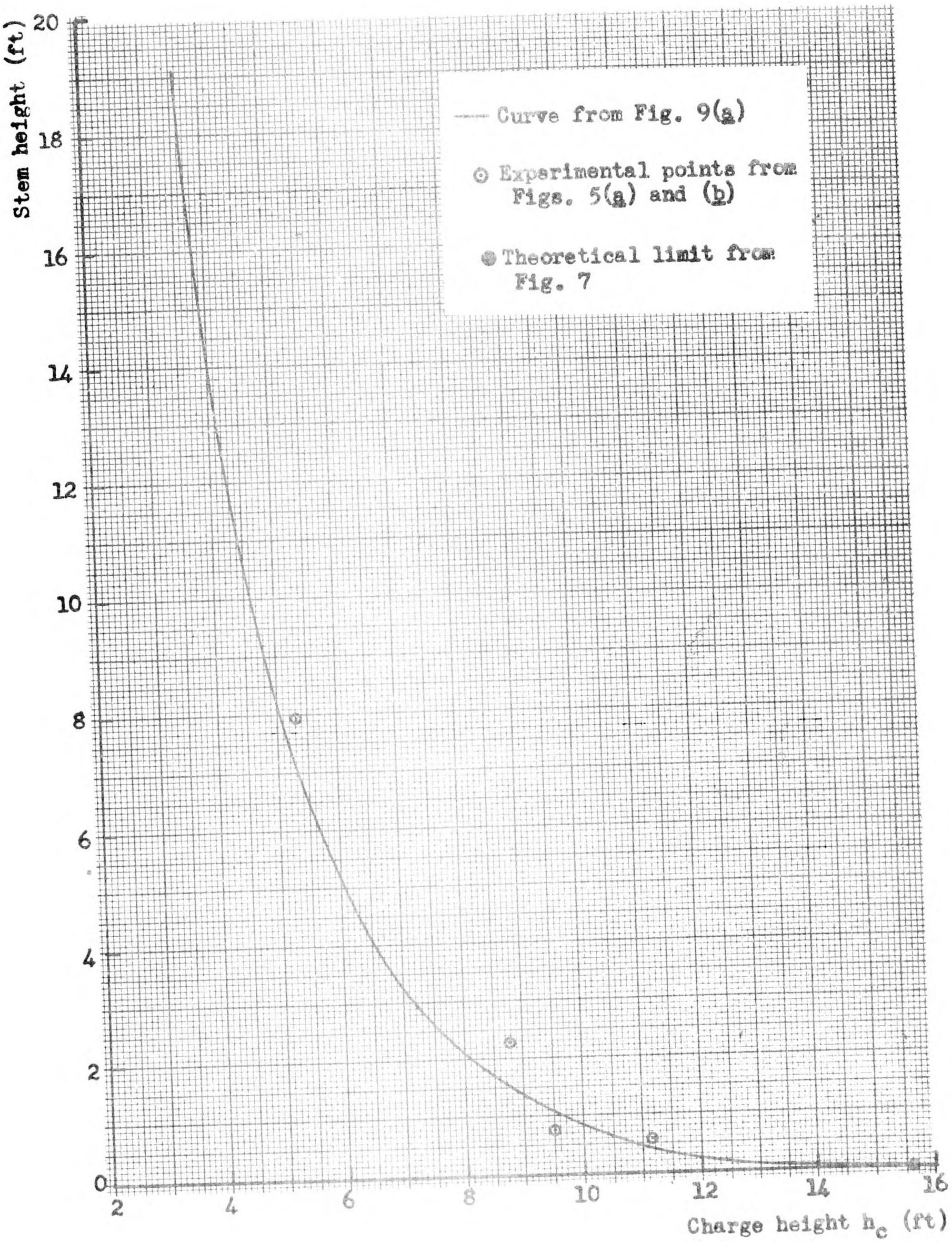

Fig. 10. Height of stem versus height of charge.
All units reduced to basis of 1 lb TNT.

Typical Pictures of Mach Shock Configuration from 500 lb. G.P. Bombs Detonated at a Reduced Charge Height of 0.4 ft. (From Motion Pictures taken at ca. 2500 frames per sec.)

Shot No. 41

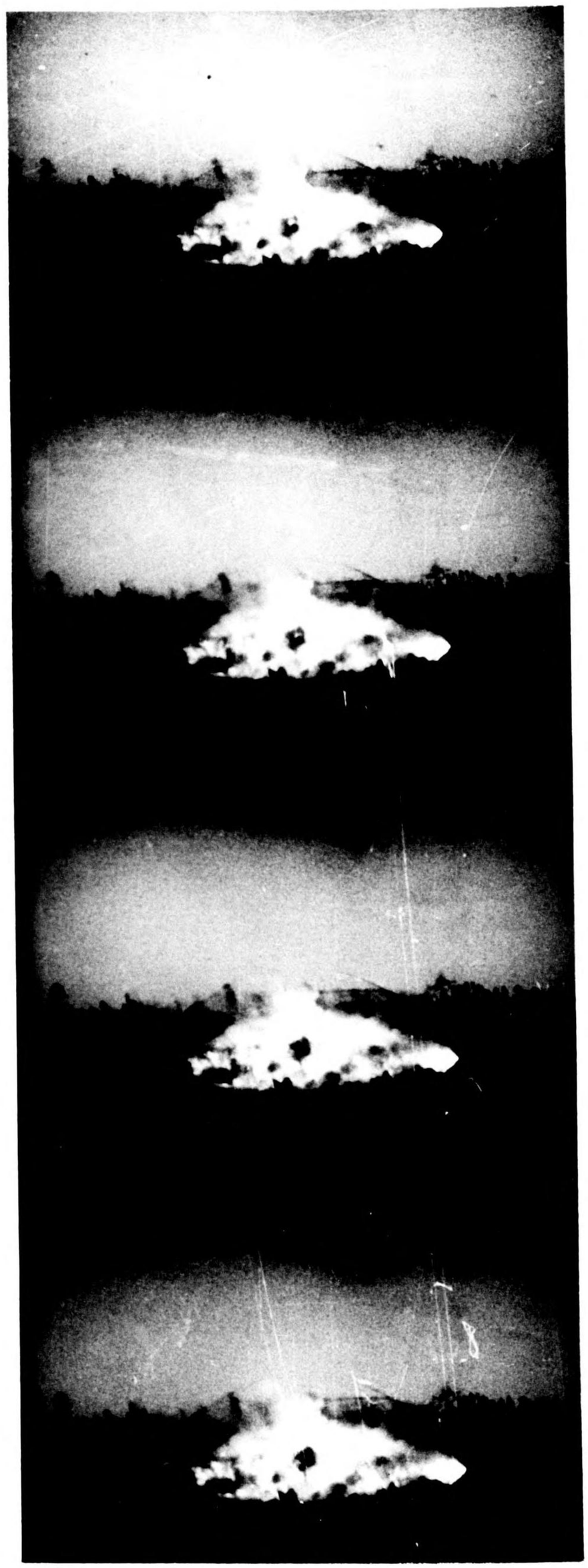

Shot No. 42

Legend for Figs. 12 through 26

Symbol	$\frac{D}{(ft)}$	Laboratory	Type Charge	Charge Weight (lb)	Reference
O	15.9	UERL	Bare GP bomb	2, 12.4, 41.7 500, 1000, 2000	1
σ	15.9	UERL	Bare (low gauges)	4.15	2
□	10.4	UERL	Bare GP bomb	12.4, 41.7 500, 1000, 2000	1
x	39.8	UERL	Bare	2	1
Δ	5-10	Princeton	Bare	½	10
$\overline{\Delta}$	10-15	Princeton	Bare	½	10
▲	15-20	Princeton	Bare	½	10
▽	20-25	Princeton	Bare	½	10
$\underline{\nabla}$	25-30	Princeton	Bare	½	10
▼	30-35	Princeton	Bare	½	10

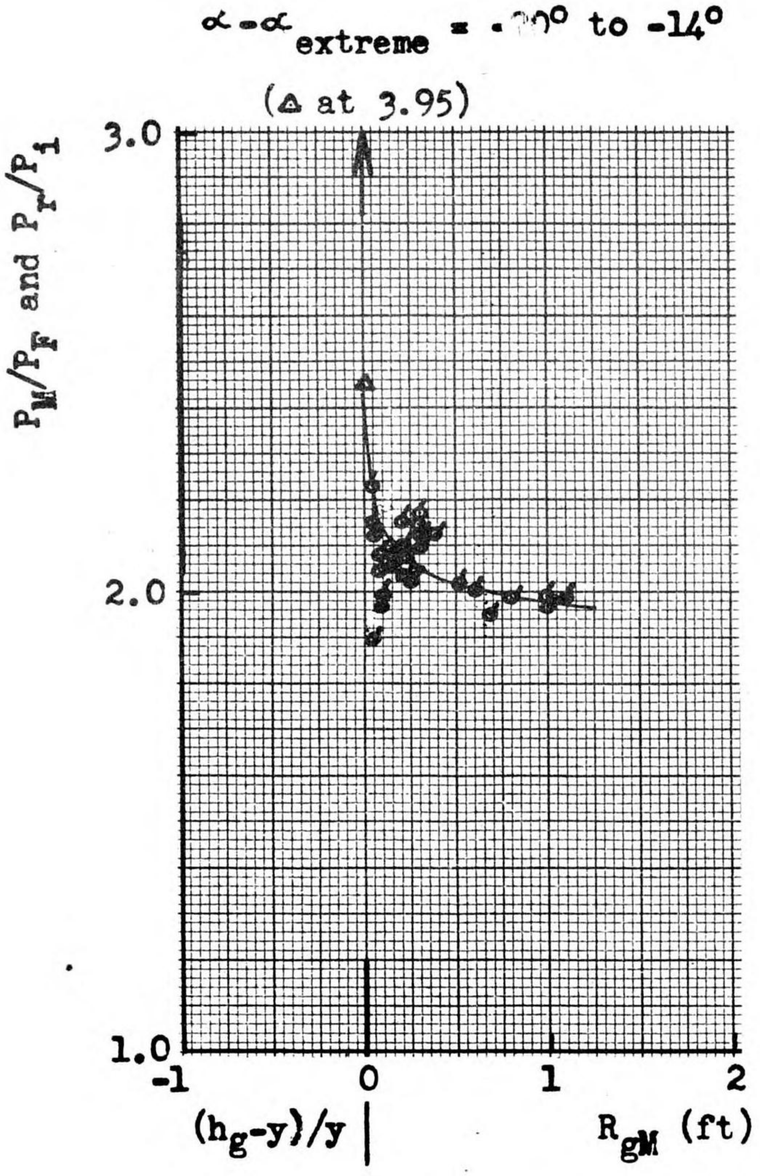

Fig. 12.

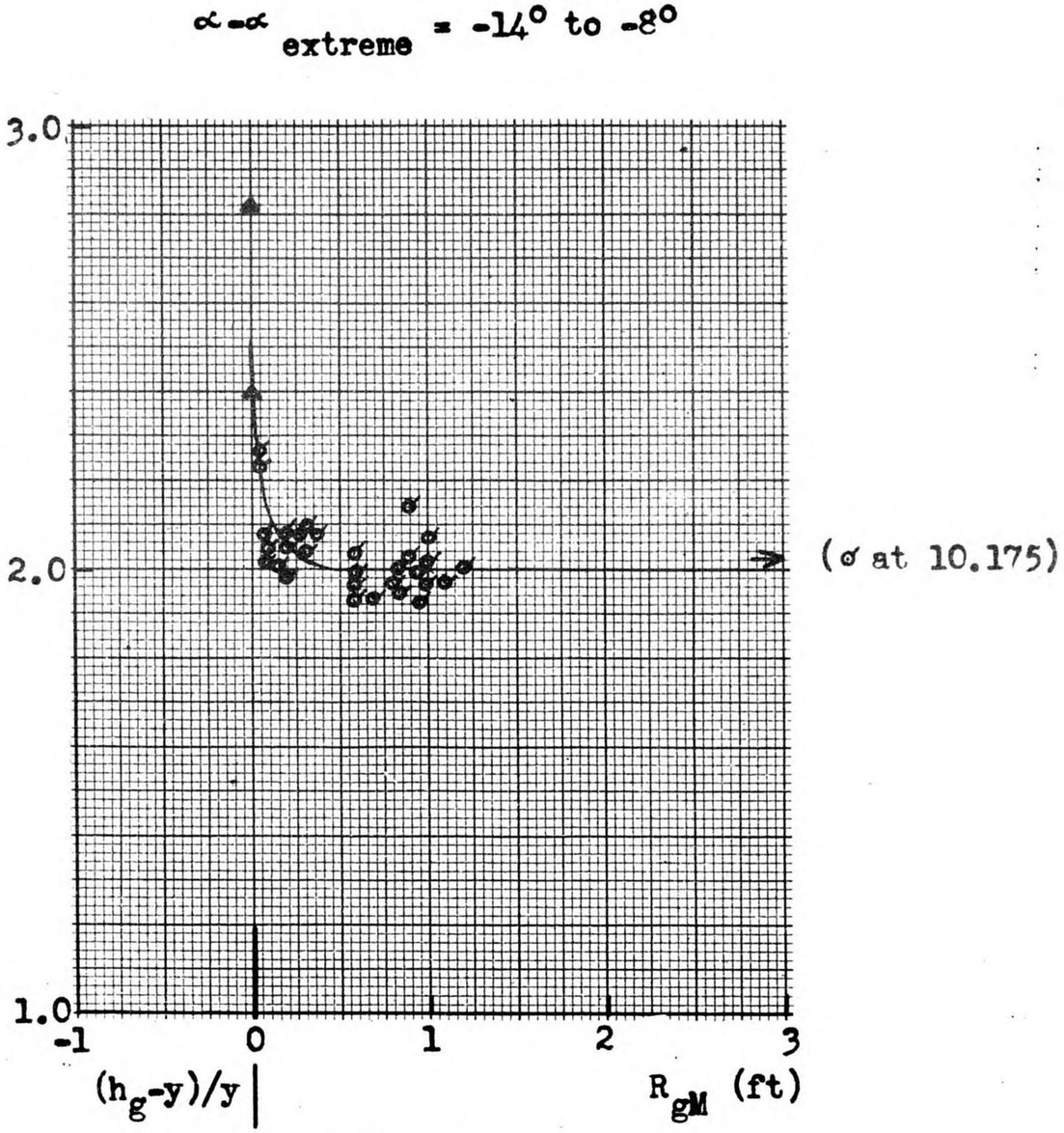

Fig. 13.

Figs. 12-13. P_r/P_i versus R_{gM} (gauges above triple point) and P_M/P_F versus $(h_g - y)/y$ (gauges below triple point).

All units reduced to basis of 1 lb TNT.

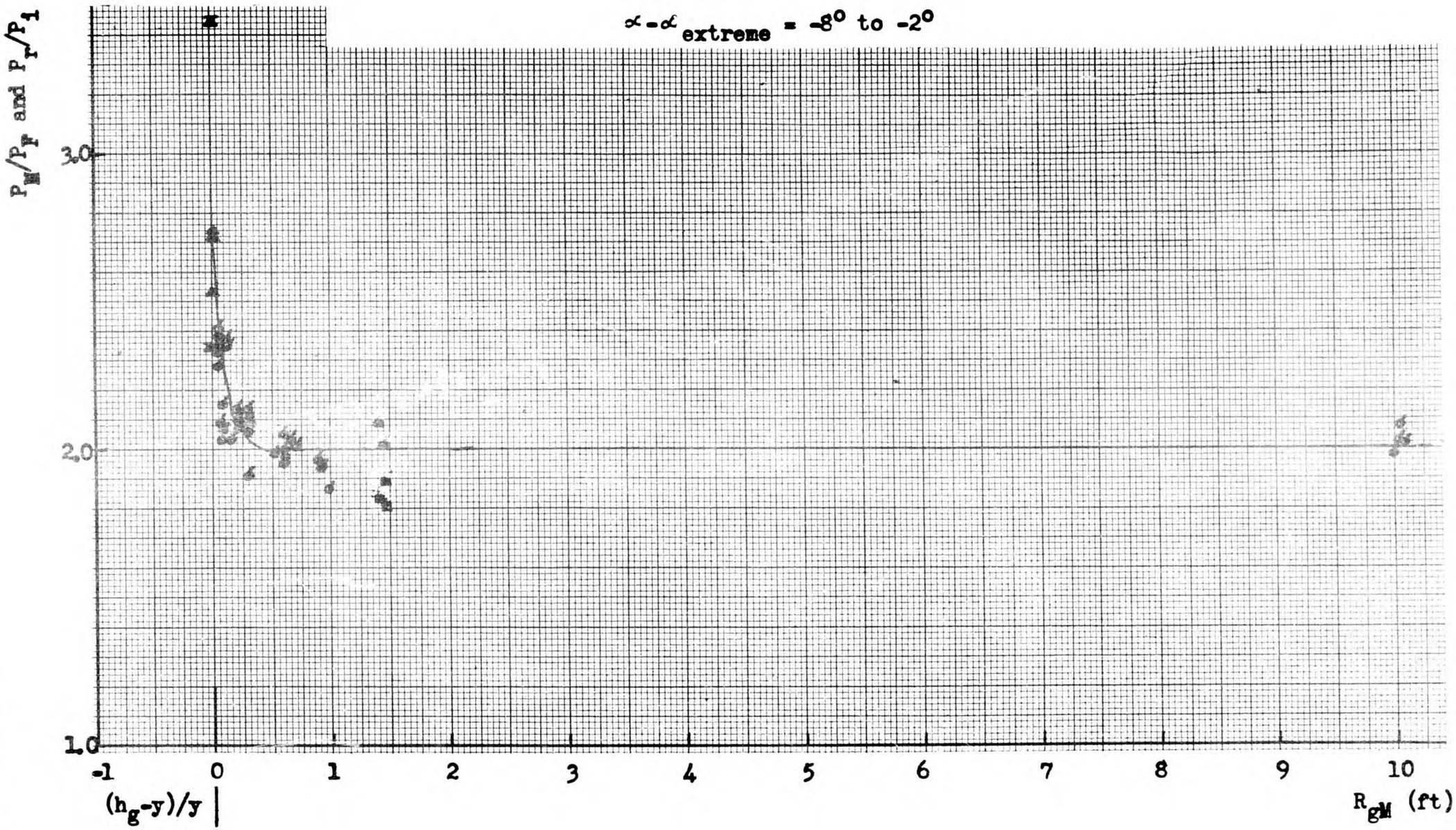

Fig. 14. P_r/P_i versus R_{gM} (gauges above triple point) and P_M/P_F versus $(h_g - y)/y$ (gauges below triple point). All units reduced to basis of 1 lb TNT.

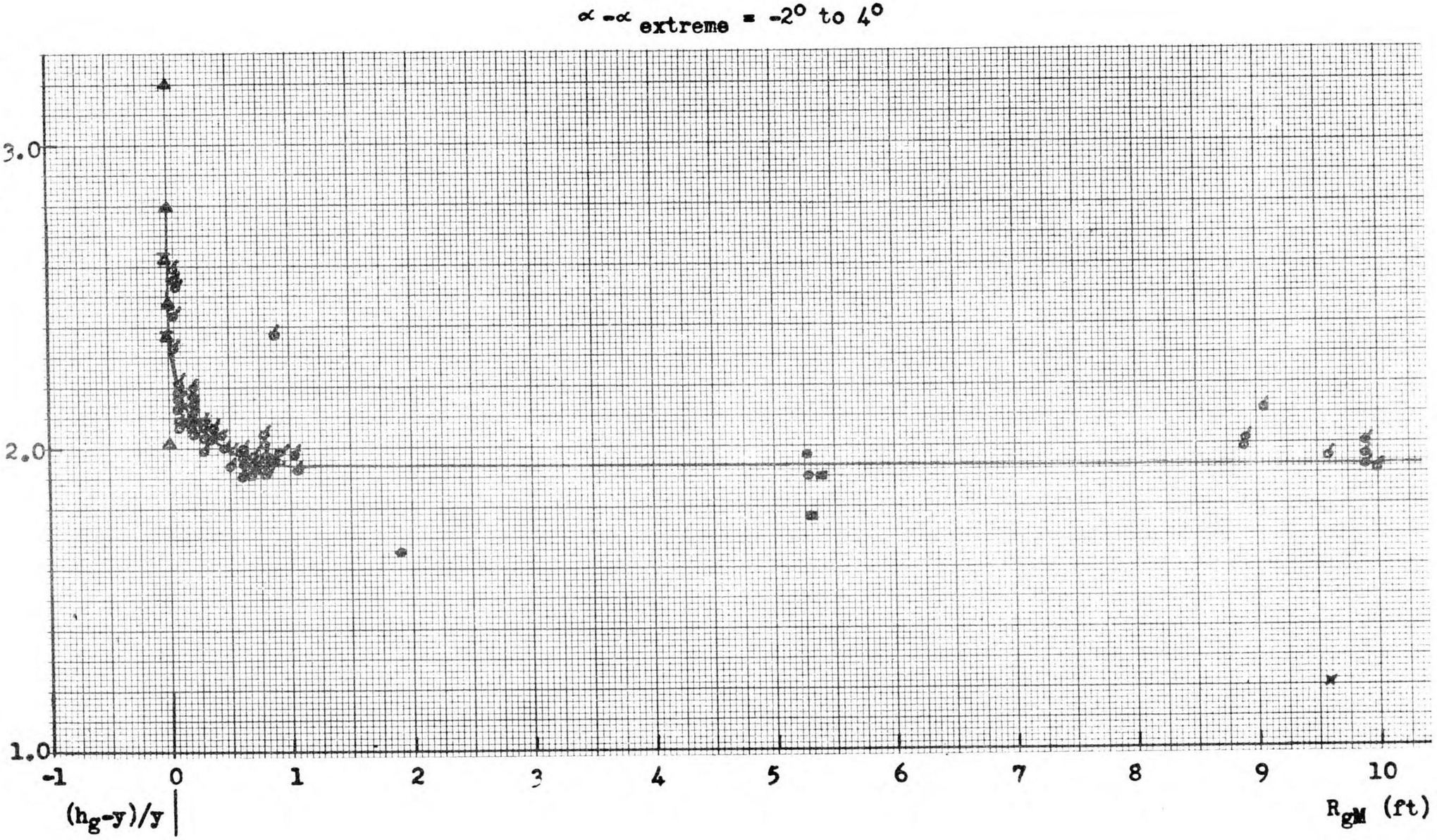

Fig. 15. P_r/P_i versus R_{gM} (gauges above triple point) and P_M/P_F versus $(h_g - y)/y$ (gauges below triple point). All units reduced to basis of 1 lb TNT.

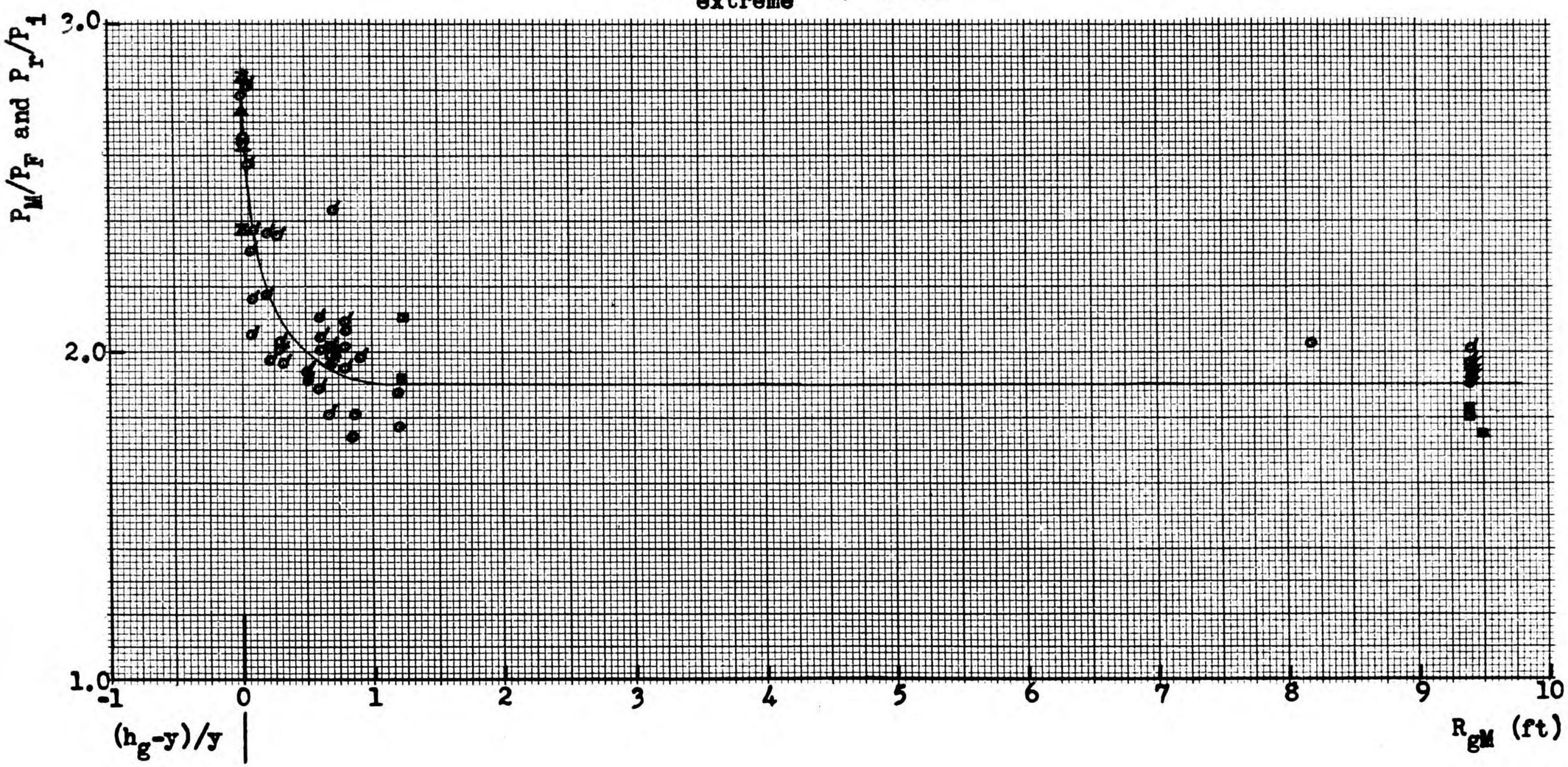

Fig. 16. P_r/P_i versus R_{gM} (gauges above triple point) and P_M/P_F versus $(h_g - y)/y$ (gauges below triple point). All units reduced to basis of 1 lb TNT.

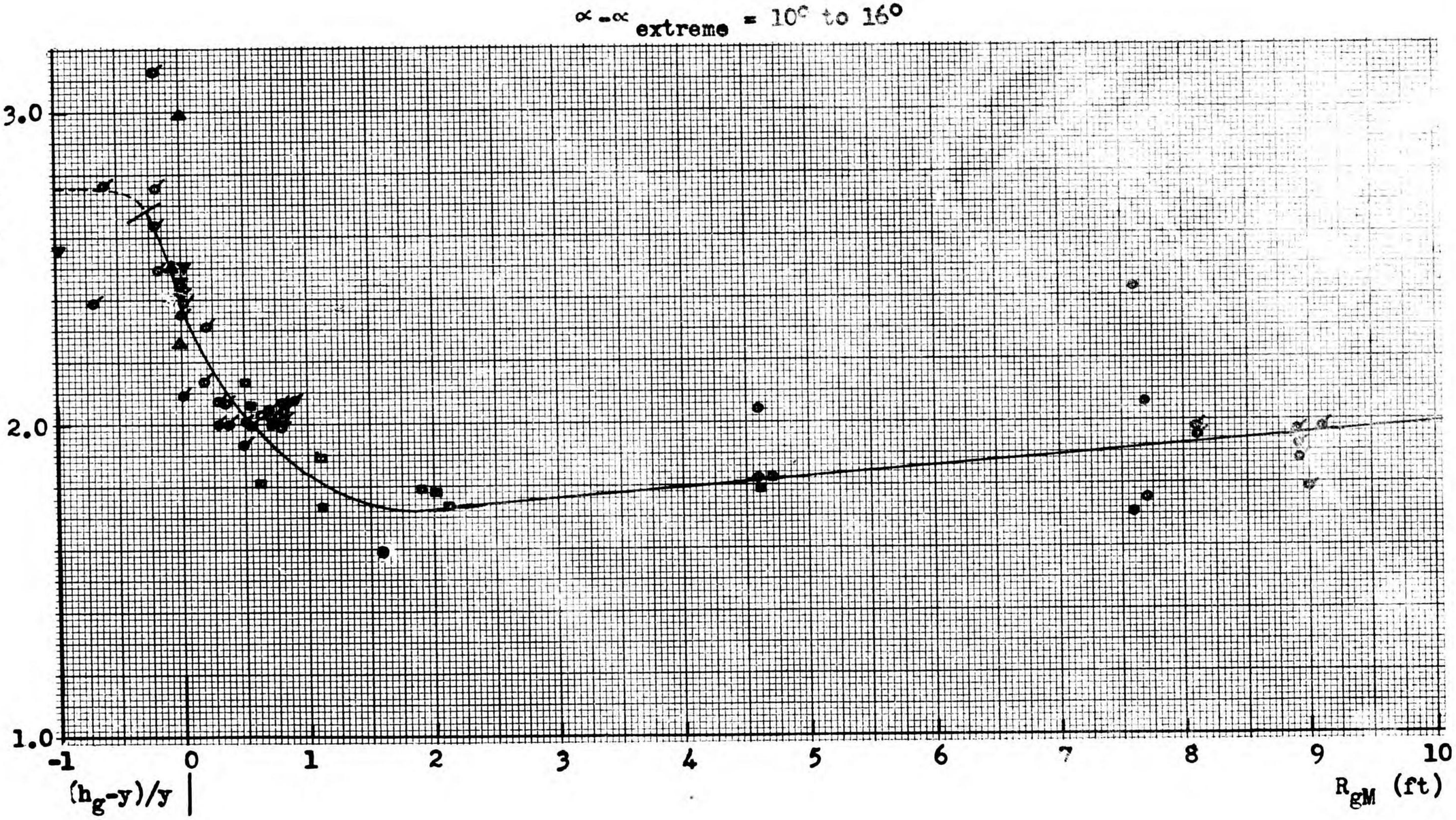

Fig. 17. P_r/P_i versus R_{gM} (gauges above triple point) and P_M/P_F versus $(h_g - y)/y$ (gauges below triple point). All units reduced to basis of 1 lb TNT.

CONFIDENTIAL

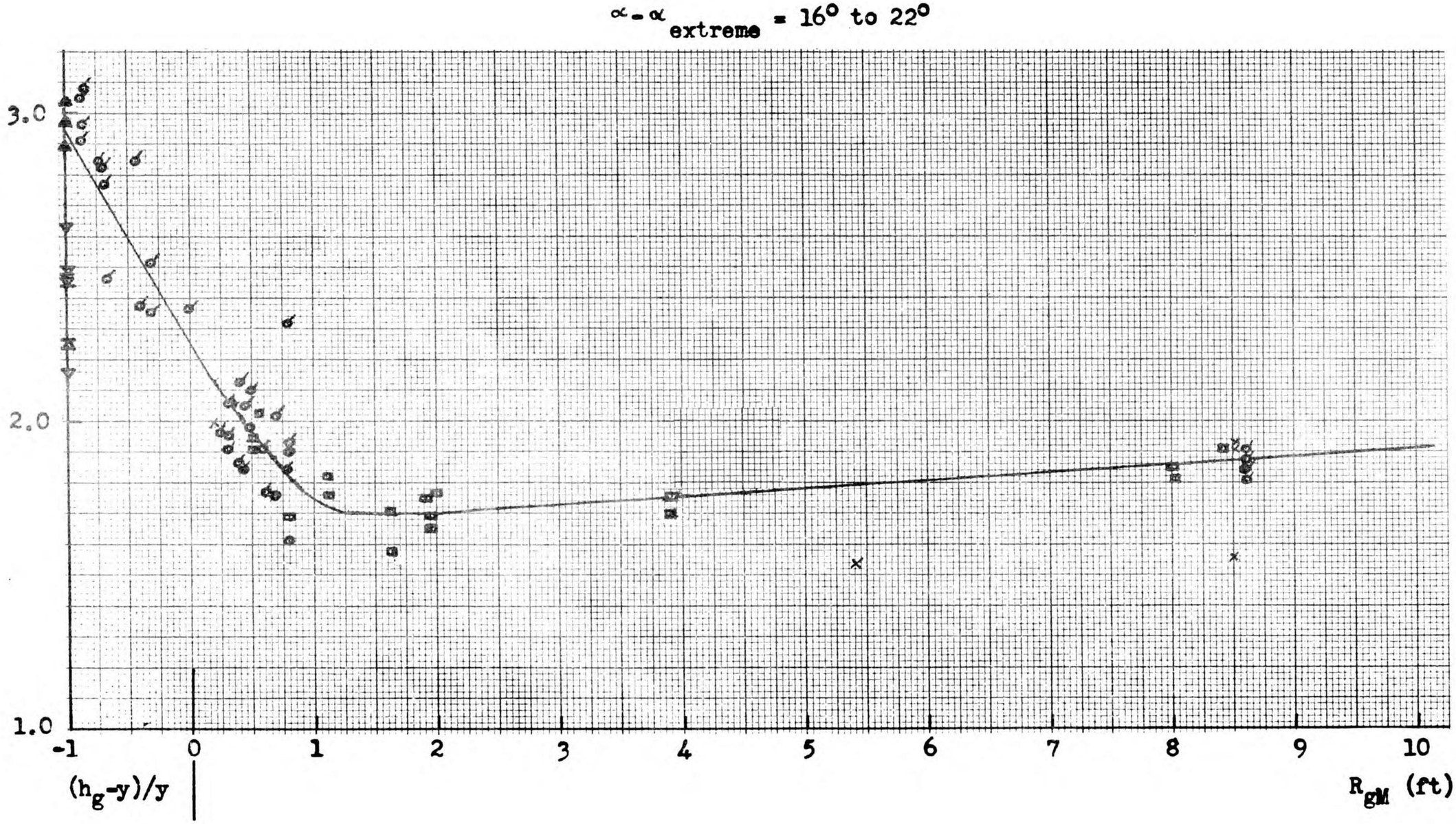

Fig. 18. P_r/P_i versus R_{gM} (gauges above triple point) and P_M/P_F versus $(h_g - y)/y$ (gauges below triple point). All units reduced to basis of 1 lb TNT.

CONFIDENTIAL

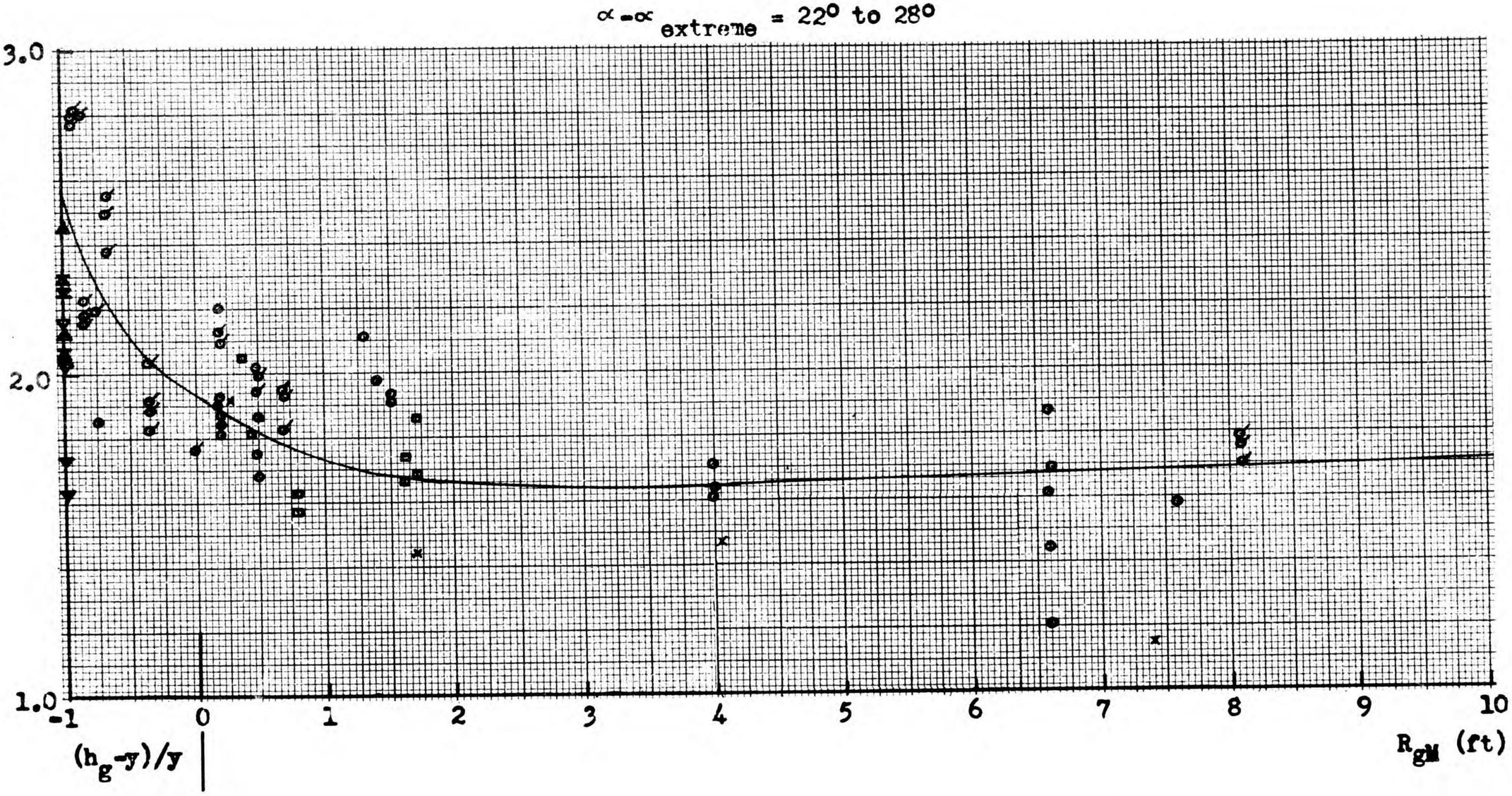

Fig. 19. P_r/P_i versus R_{gM} (gauges above triple point) and P_M/P_F versus $(h_g - y)/y$ (gauges below triple point). All units reduced to basis of 1 lb TNT.

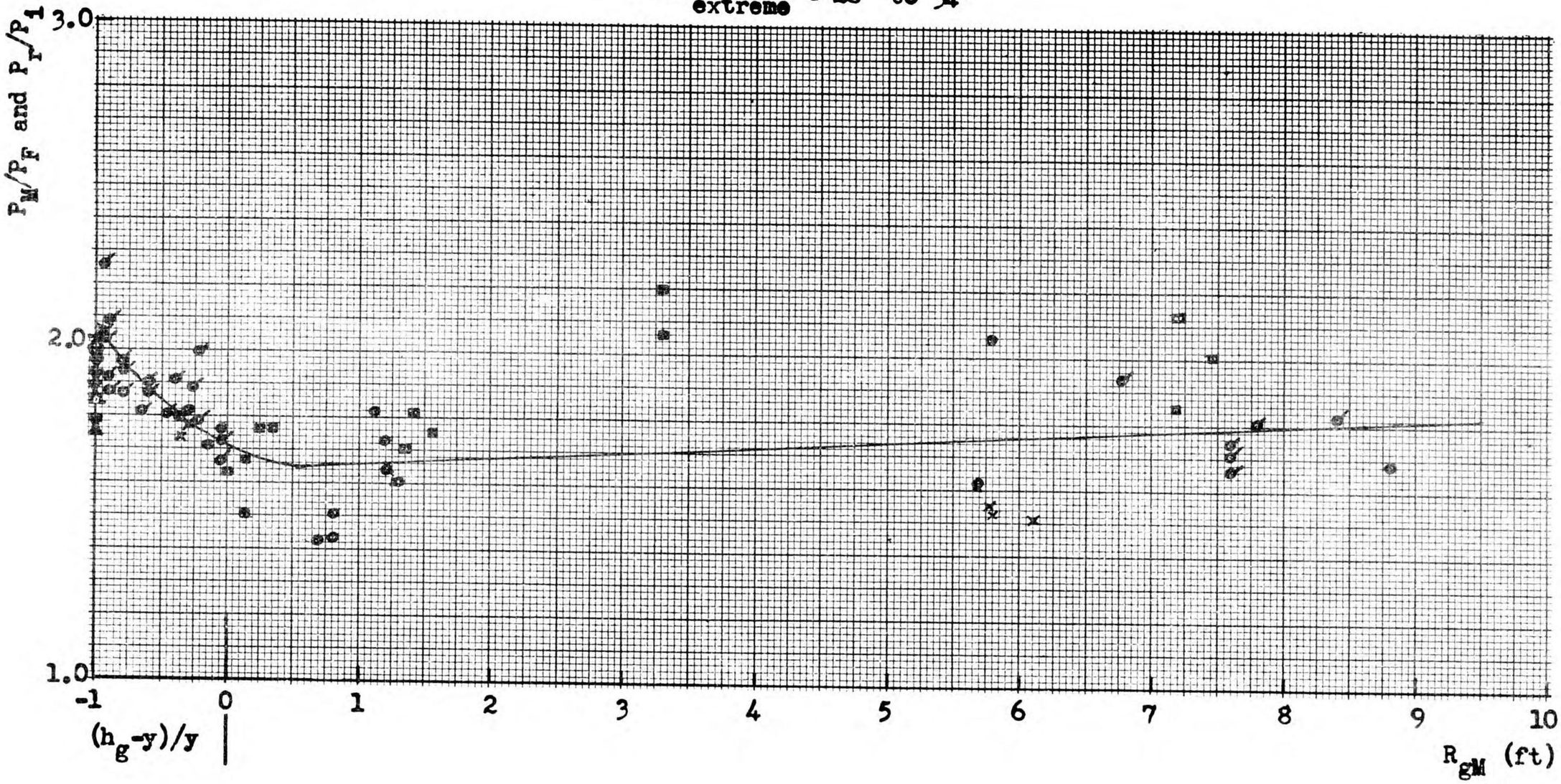

Fig. 20. P_r/P_i versus R_{gM} (gauges above triple point) and P_M/P_F versus $(h_g - y)/y$ (gauges below triple point). All units reduced to basis of 1 lb TNT.

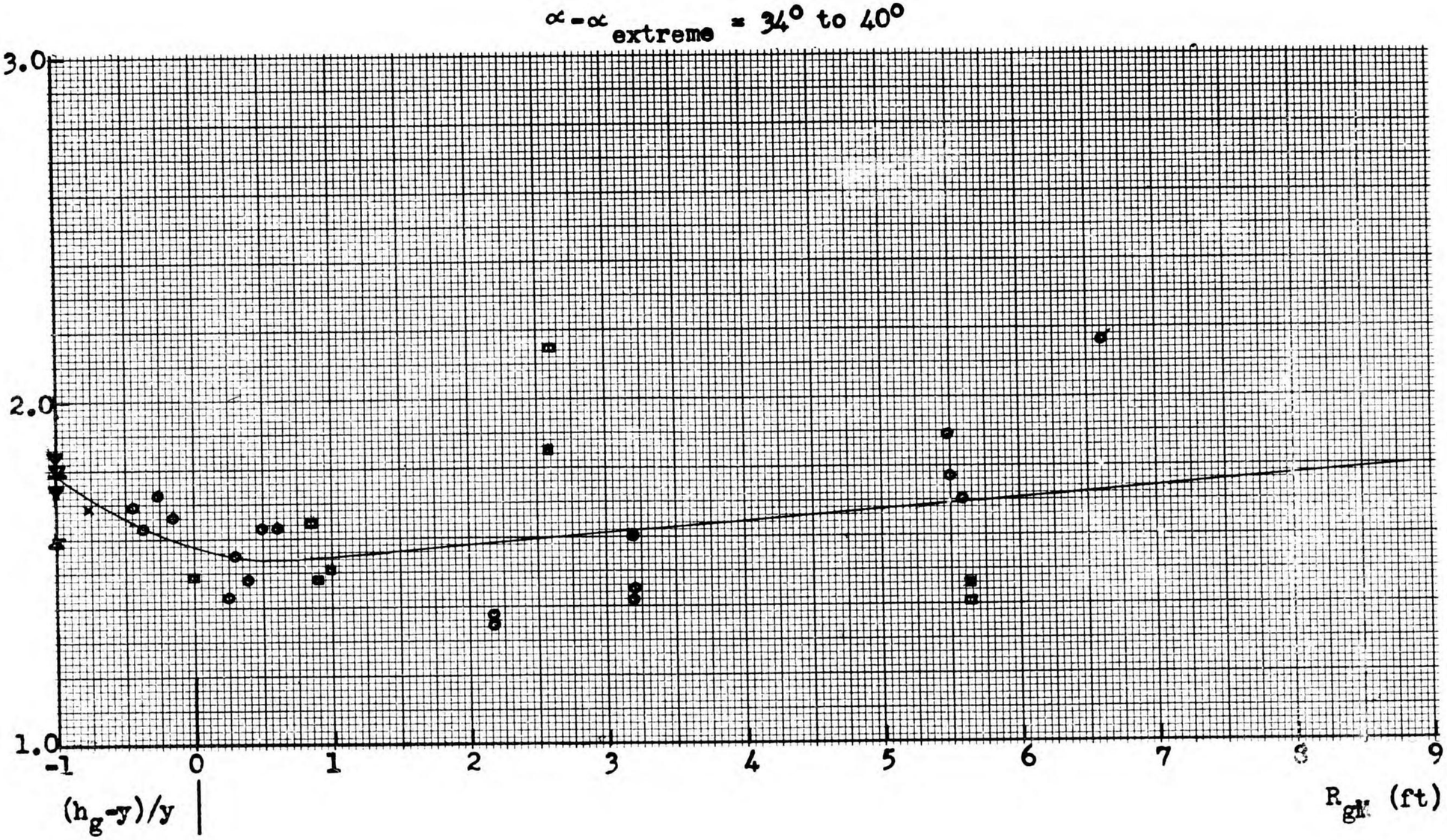

Fig. 21. P_r/P_i versus R_{gM} (gauges above triple point) and P_M/P_F versus $(h_g - y)/y$ (gauges below triple point).

All units reduced to basis of 1 lb TNT.

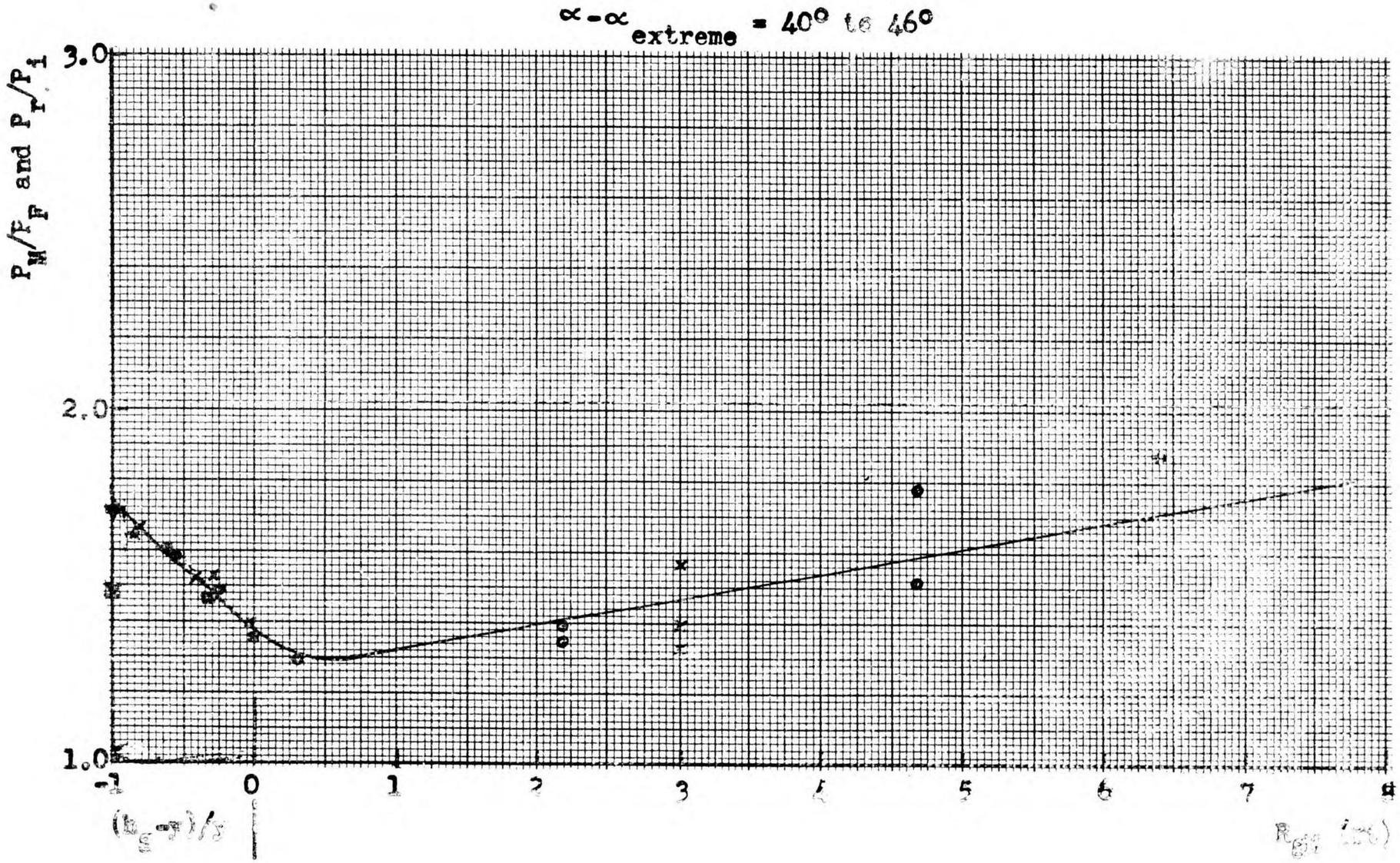

Fig. 22. P_r/P_i versus R_{gd} (gauges above triple point) and P_M/P_F versus $(h_g - 3)/3$ (gauges below triple point).

All units reduced to basis of 1 lb TNT.

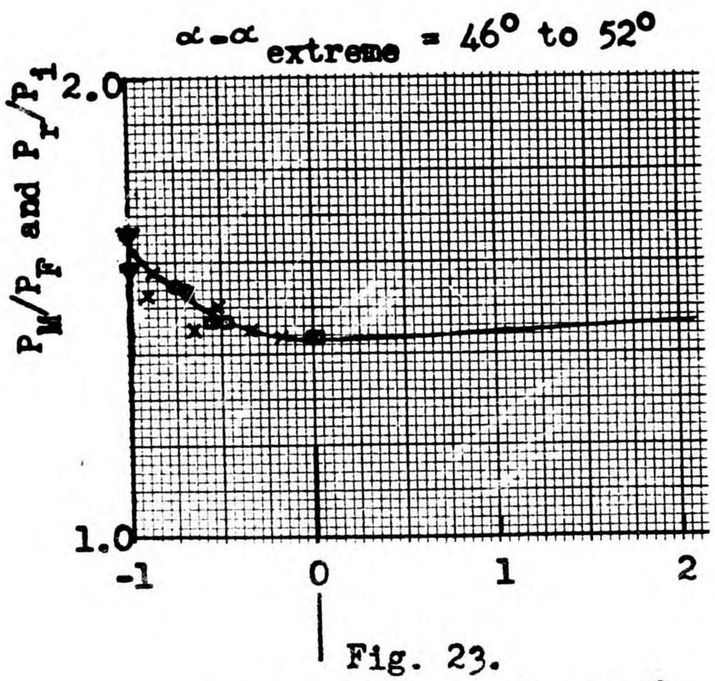

Fig. 23.

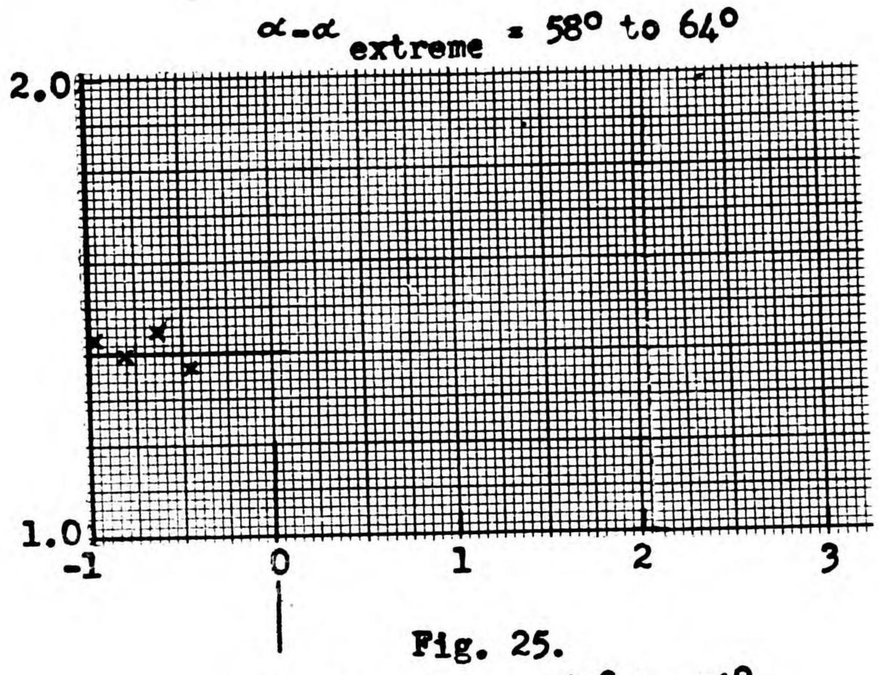

Fig. 25.

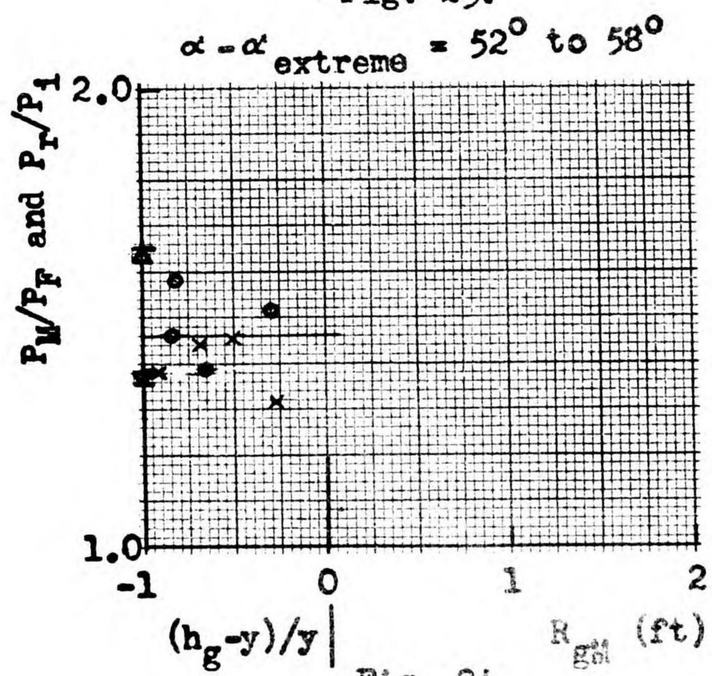

Fig. 24.

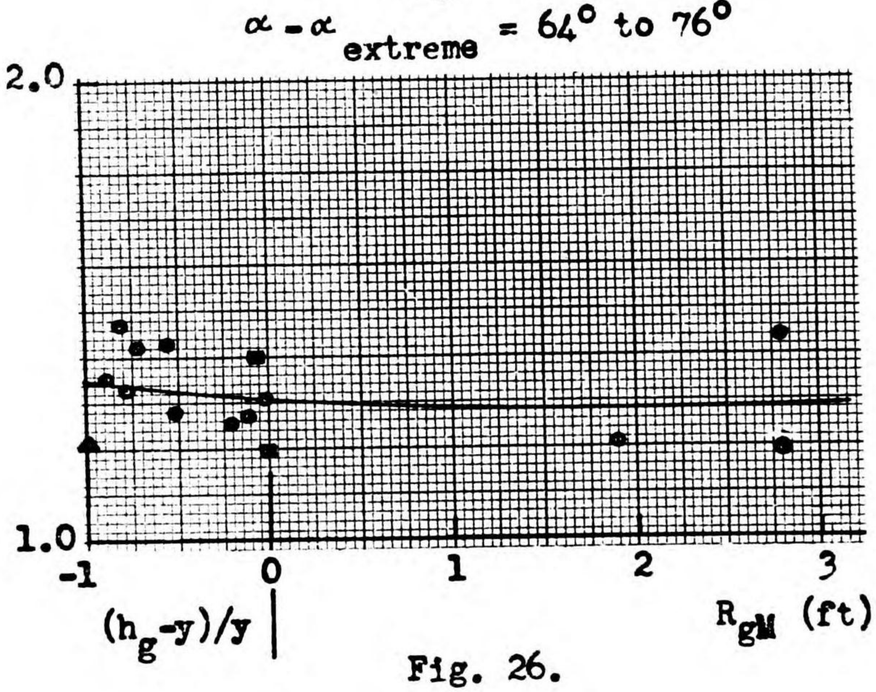

Fig. 26.

Figs. 23-26. P_r/P_i versus R_{gM} (gauges above triple point) and P_M/P_F versus $(h_g - y)/y$ (gauges below triple point).

All units reduced to basis of 1 lb TNT.

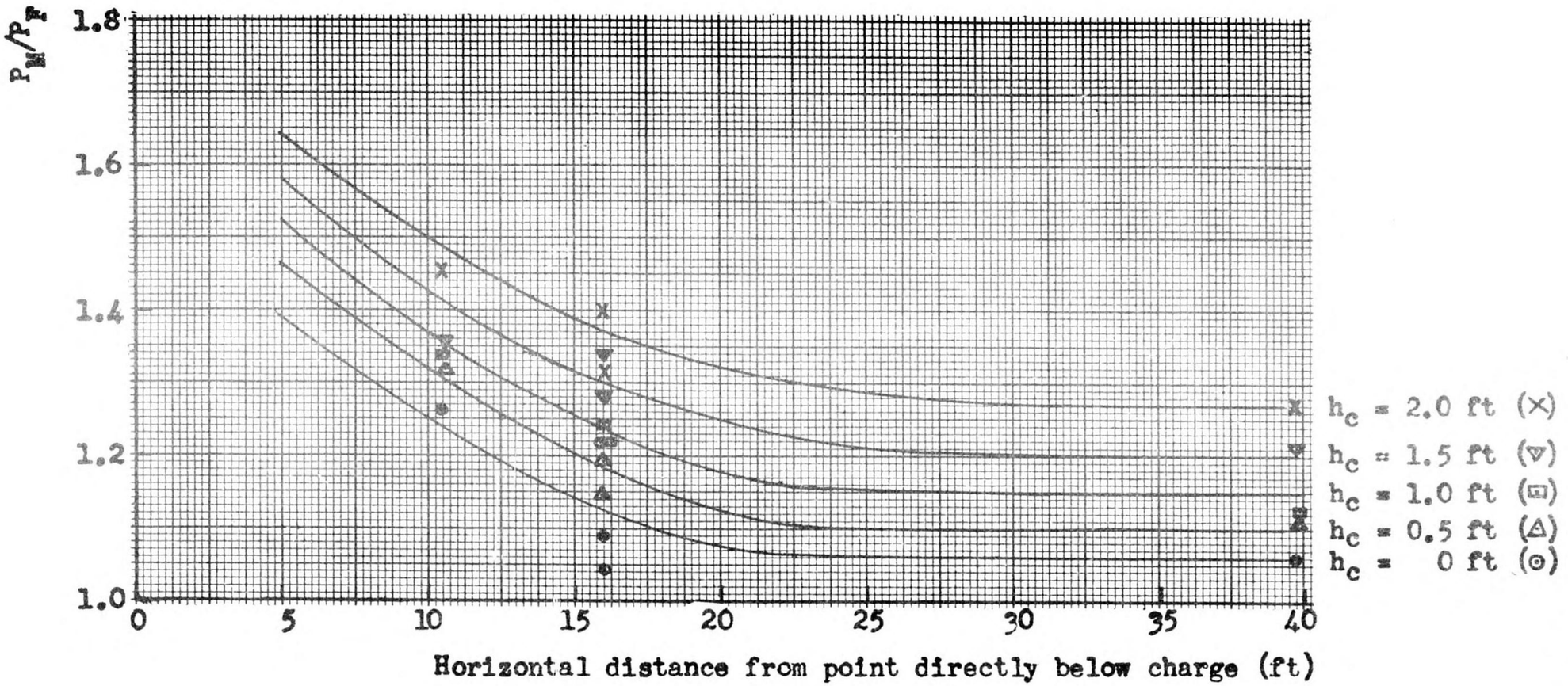

Fig. 27. P_M/P_F versus horizontal distance from charge for low charge heights. All units reduced to basis of 1 lb TNT.

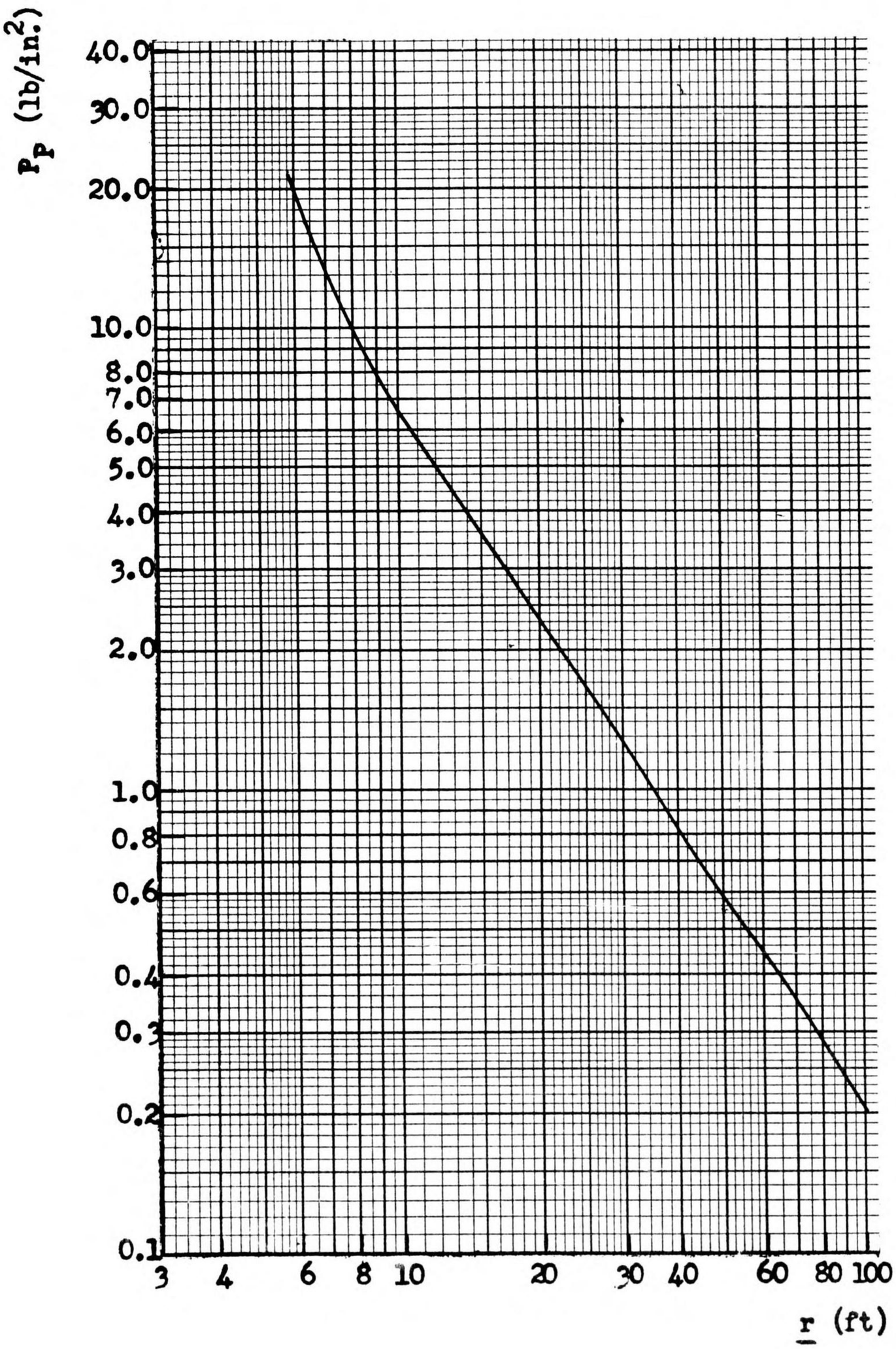

Fig. 28. Free-air peak pressure versus distance.
All units reduced to basis of 1 lb TNT.

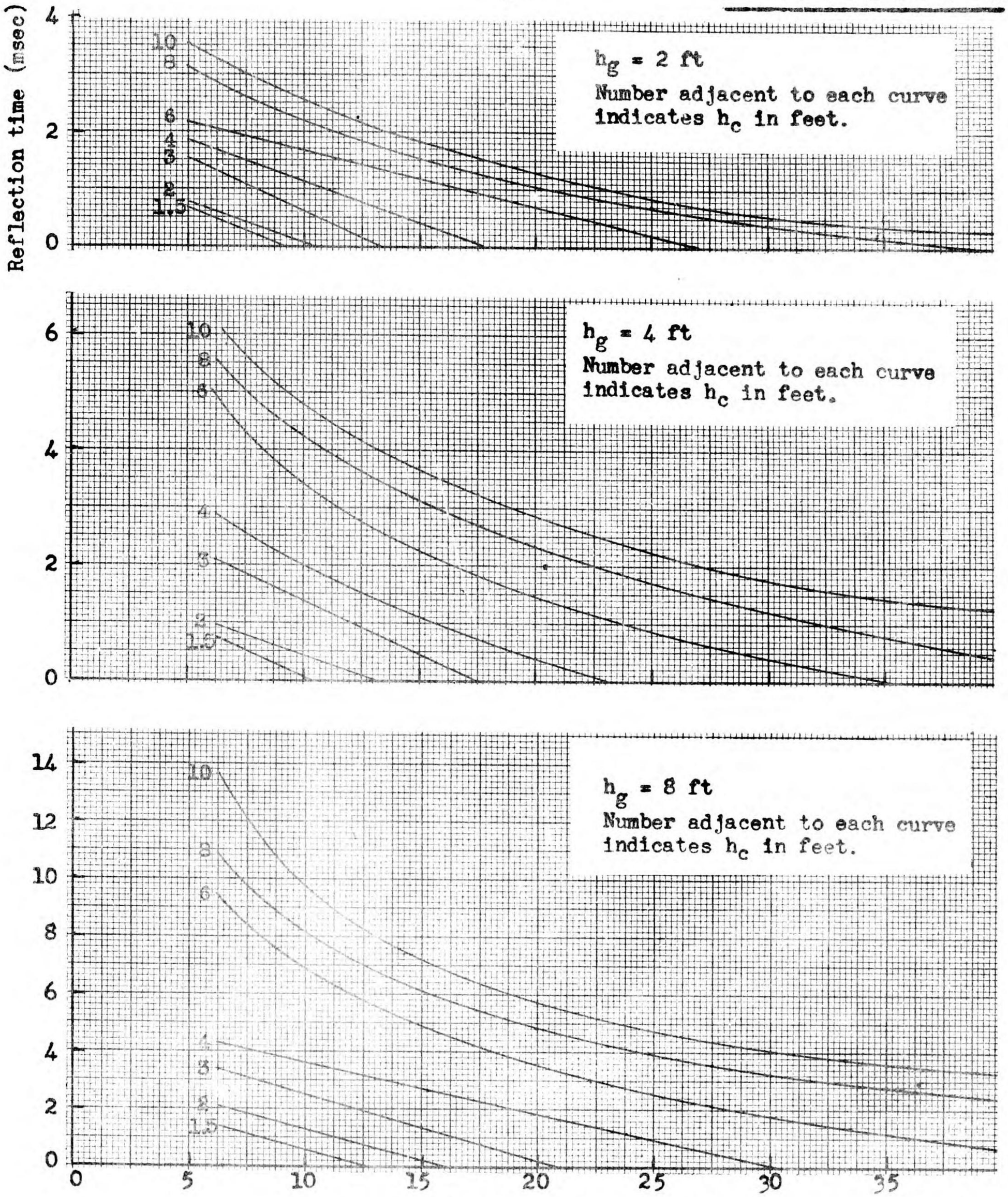

Fig. 29. Reflection time versus horizontal distance from charge for various values of charge height and gauge height.
All units reduced to basis of 1 lb TNT.

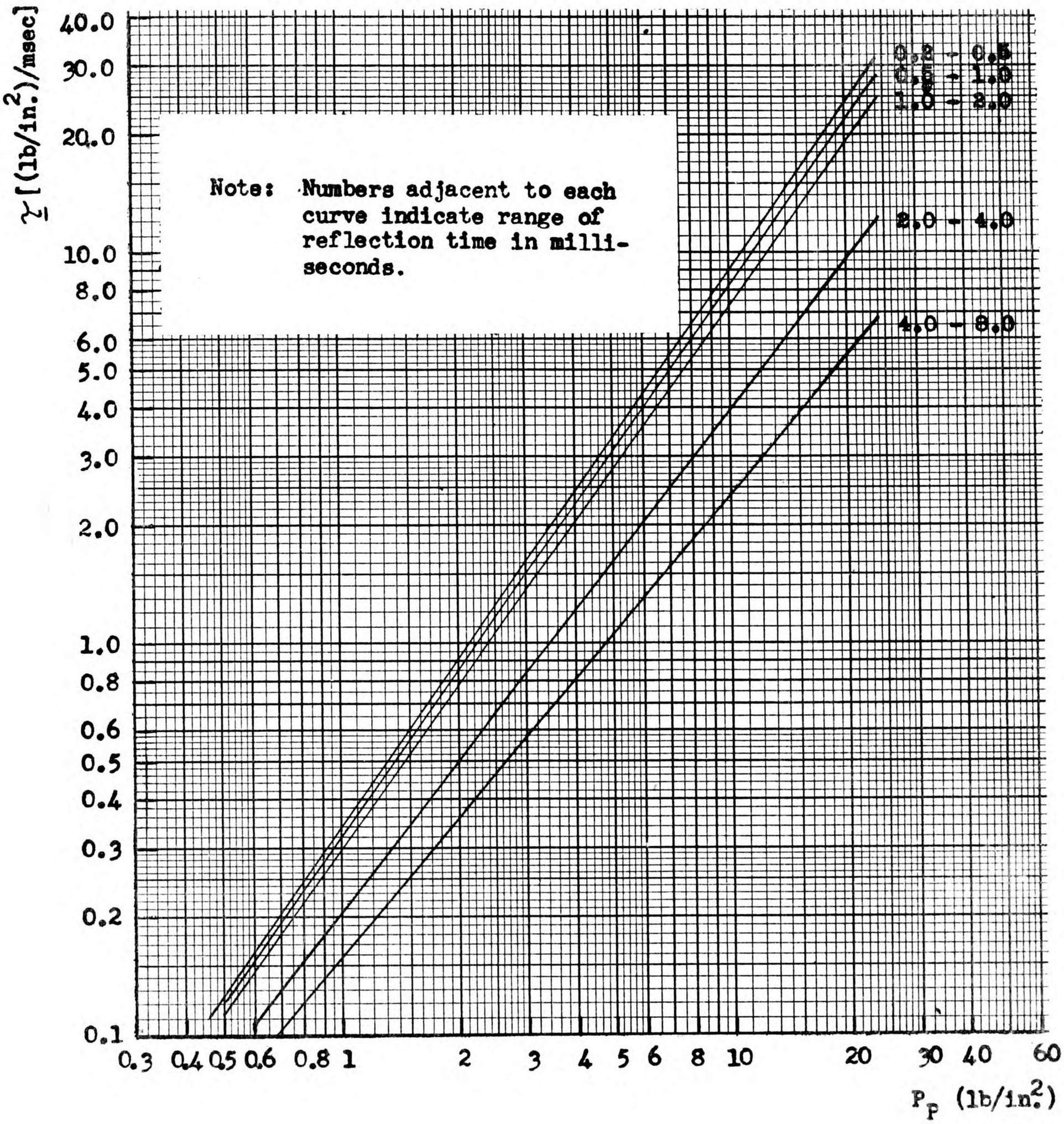

Fig. 30. Time-decay constant versus free-air peak pressure for various ranges of reflection time.
All units reduced to basis of 1 lb TNT.

Legend for Figs. 31 through 35

Symbol	Quantity	Definition	Source
□	P_M	Peak pressure of Mach shock measured by gauge in Mach region (single-peak record)	Calculated from Figs. 12-28.
○	P_P	Peak pressure of incident shock for gauge outside Mach region (double-peak record)	Taken from Fig. 28.
Δ	P_R	Peak pressure of reflected or second shock on double-peak record	Calculated from Figs. 12-30.
x	P_M	Peak pressure of Mach shock measured by gauge in Mach region (single-peak record)	Taken from Ref. 10 for $h_g = 0$.

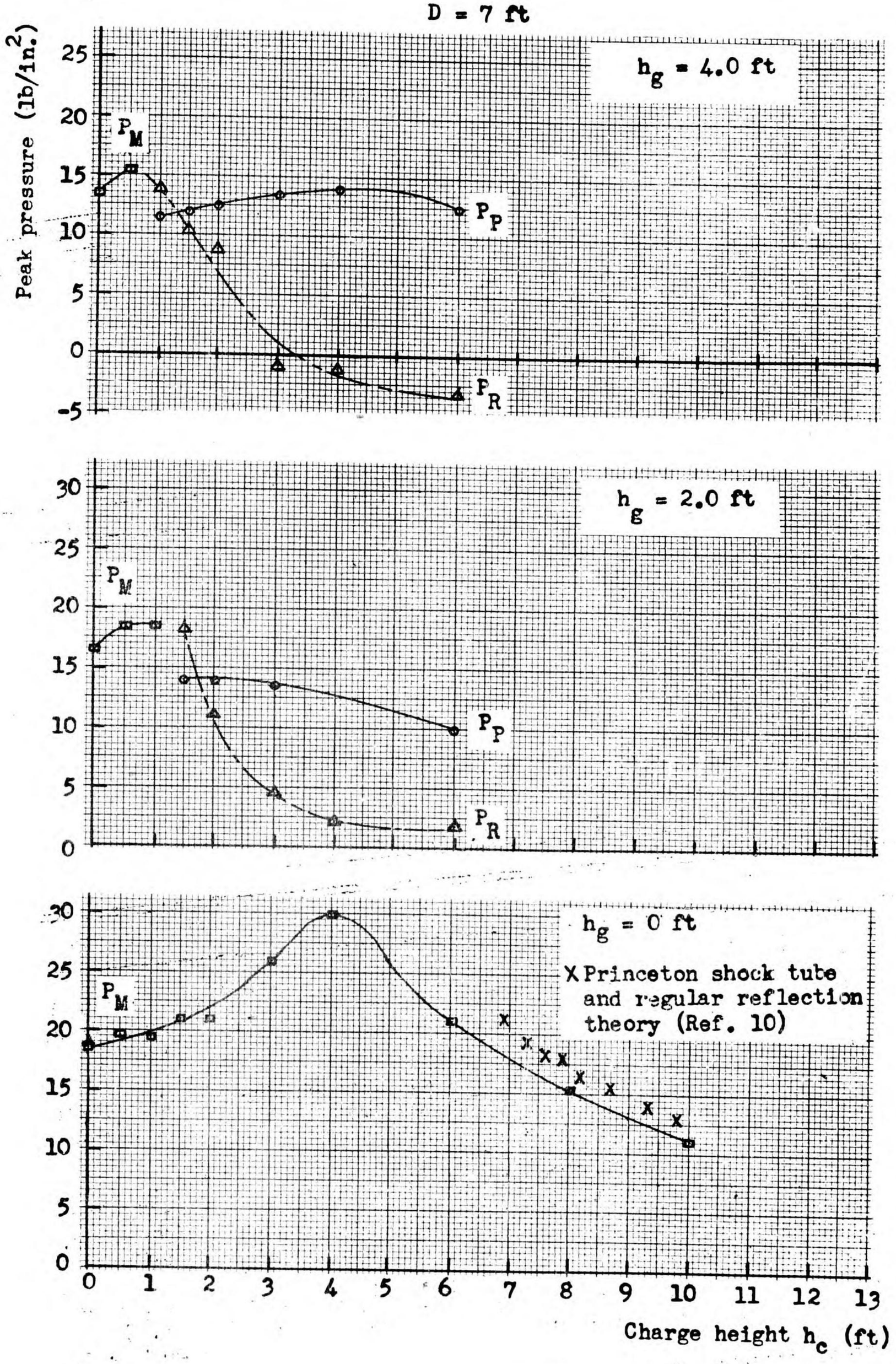

Fig. 31. Predicted pressure versus charge height.
All units reduced to basis of 1 lb TNT.

D = 10 ft

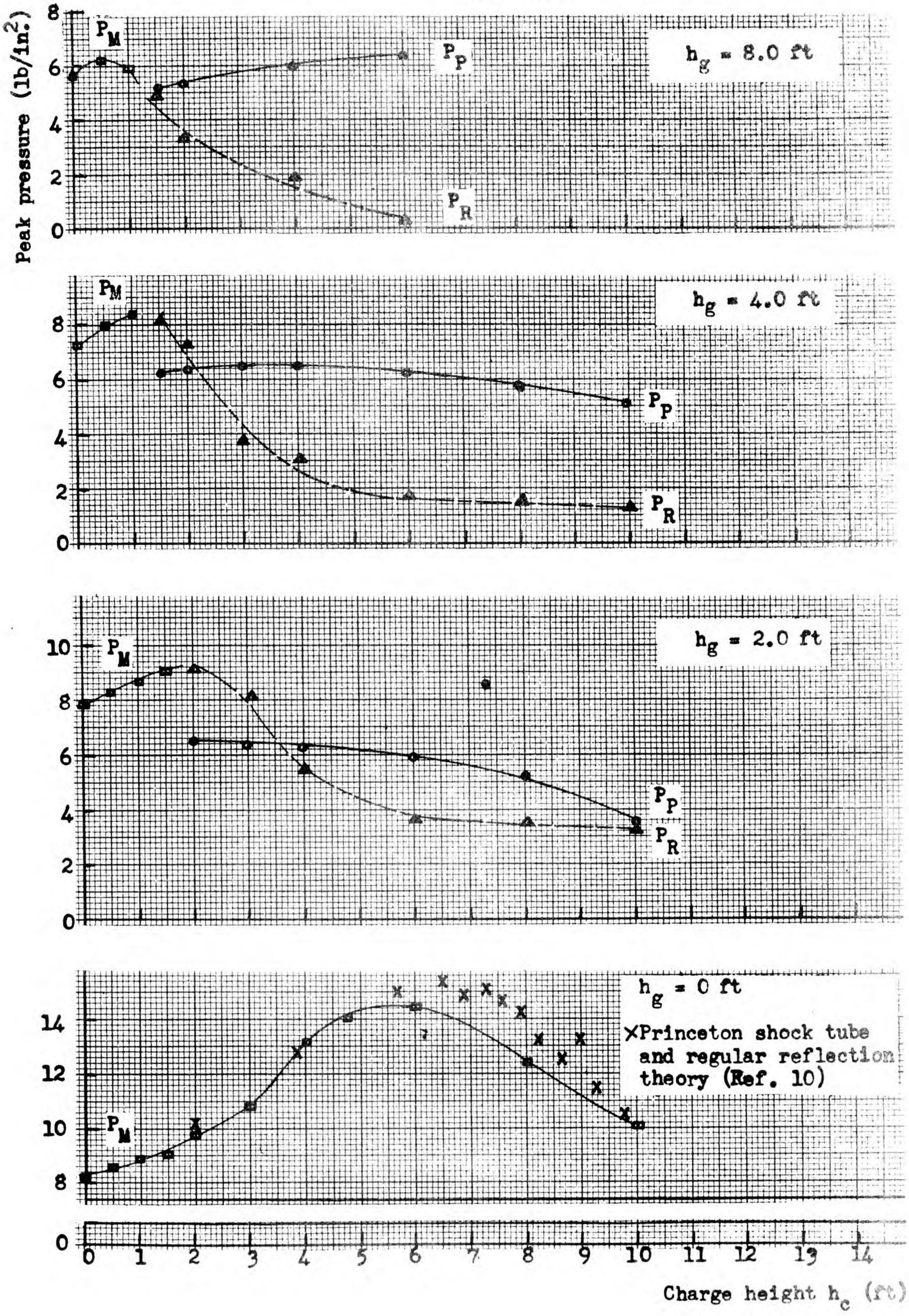

Fig. 32. Predicted pressure versus charge height.
All units reduced to basis of 1 lb TNT.

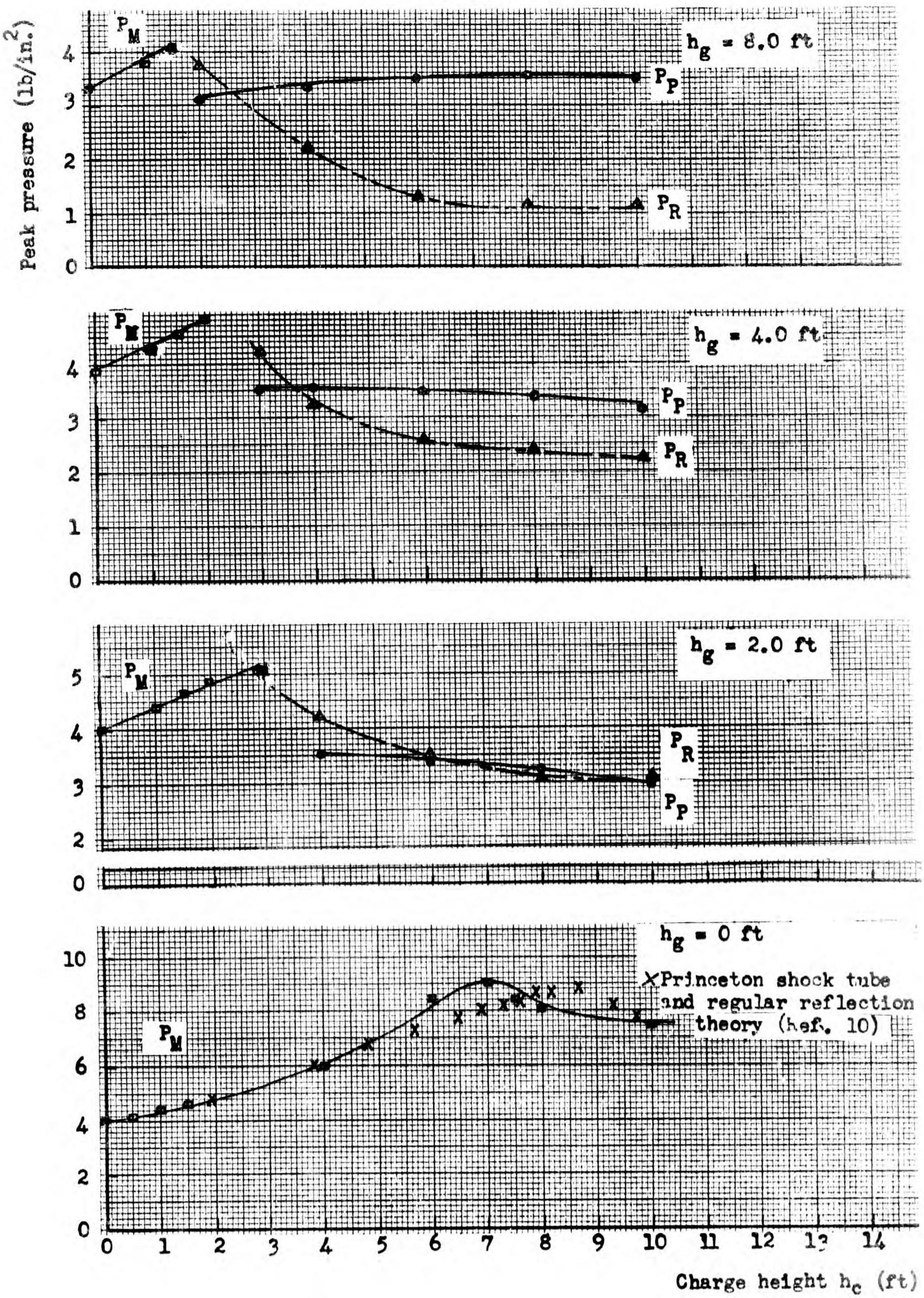

Fig. 23. Predicted pressure versus charge height.
All units reduced to basis of 1 lb TNT.

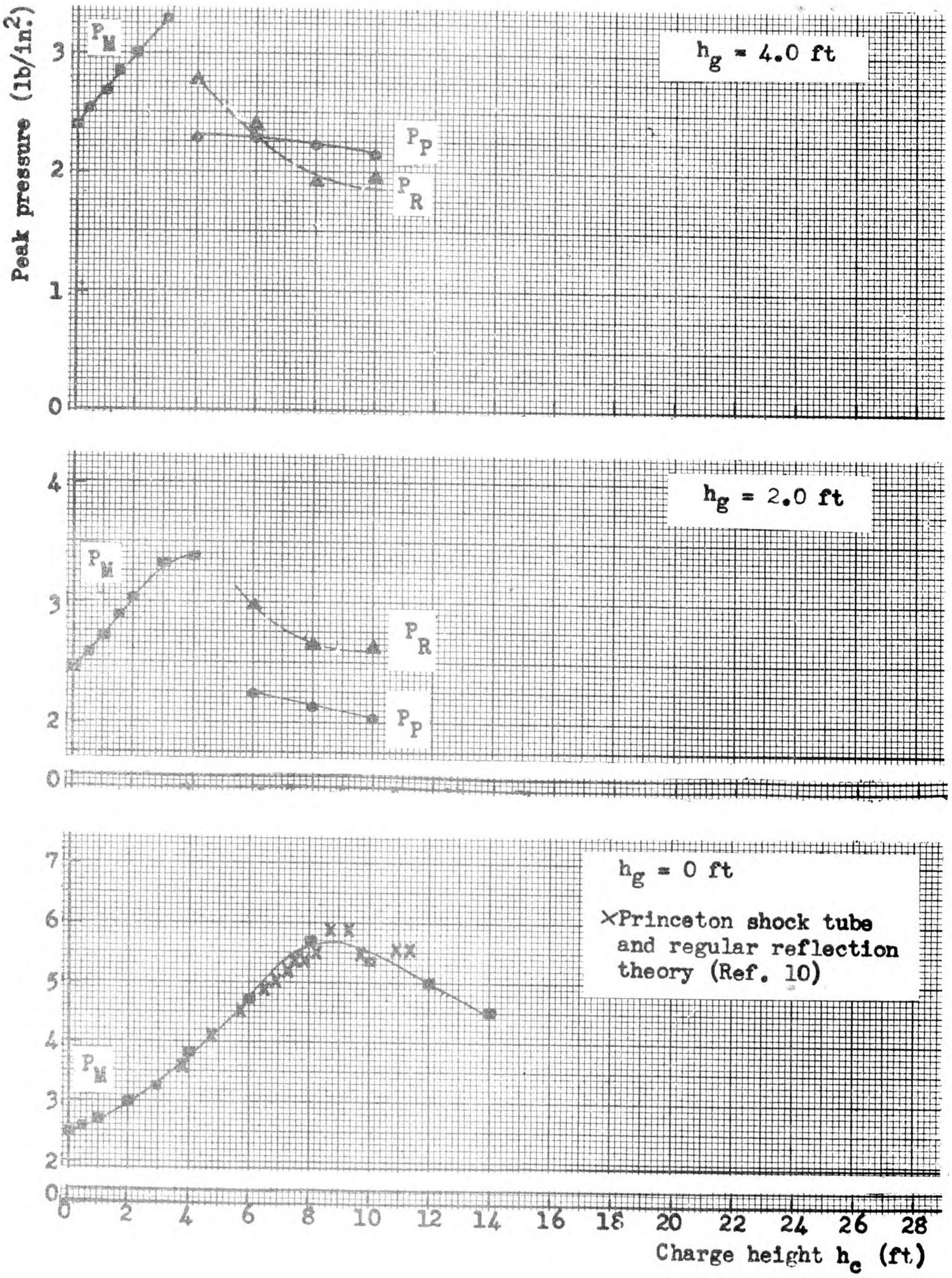

Fig. 34. Predicted pressure versus charge height.
All units reduced to basis of 1 lb TNT.

D = 40 ft

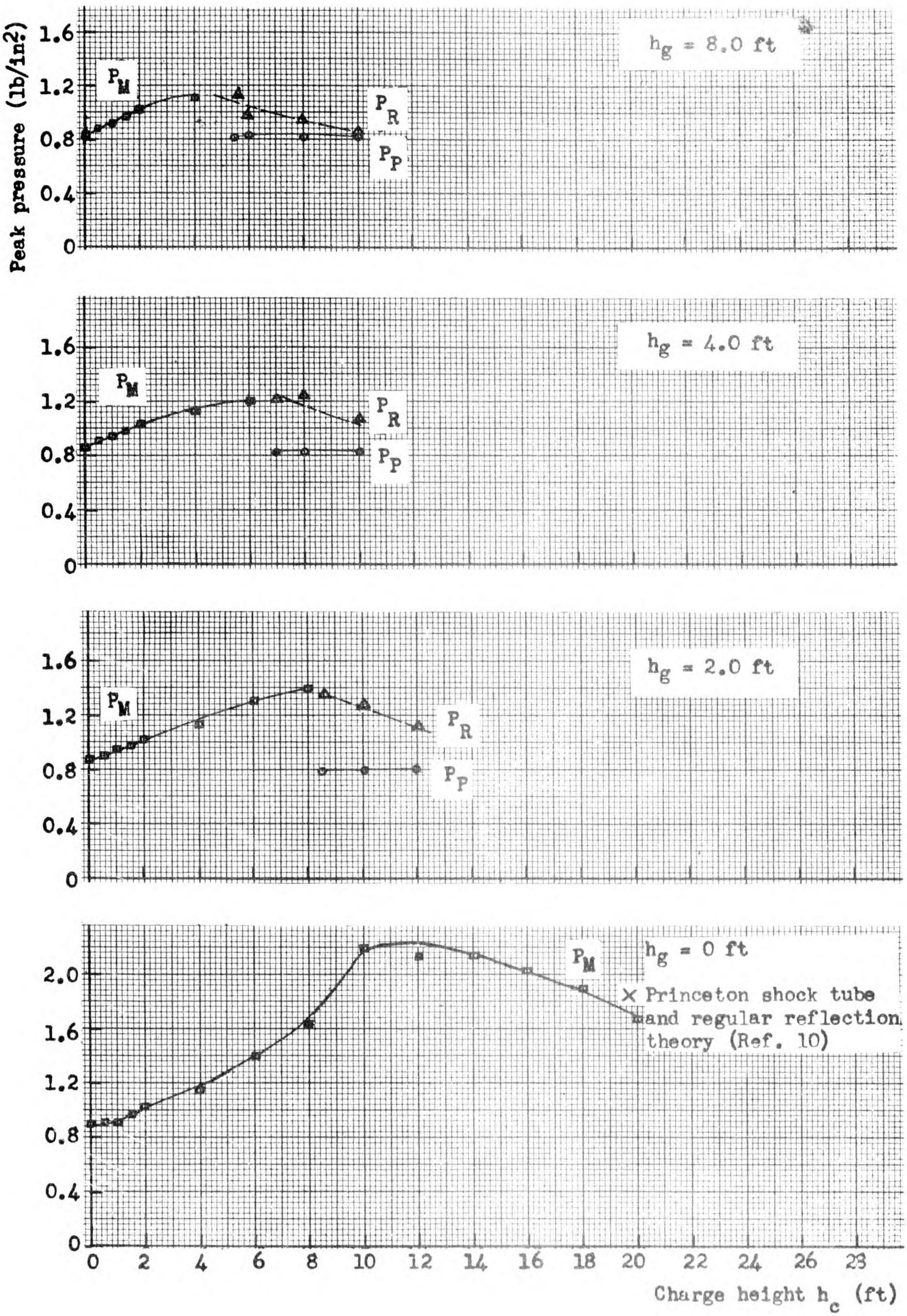

Fig. 35. Predicted pressure versus charge height.
All units reduced to basis of 1 lb TNT.

Averaged over D

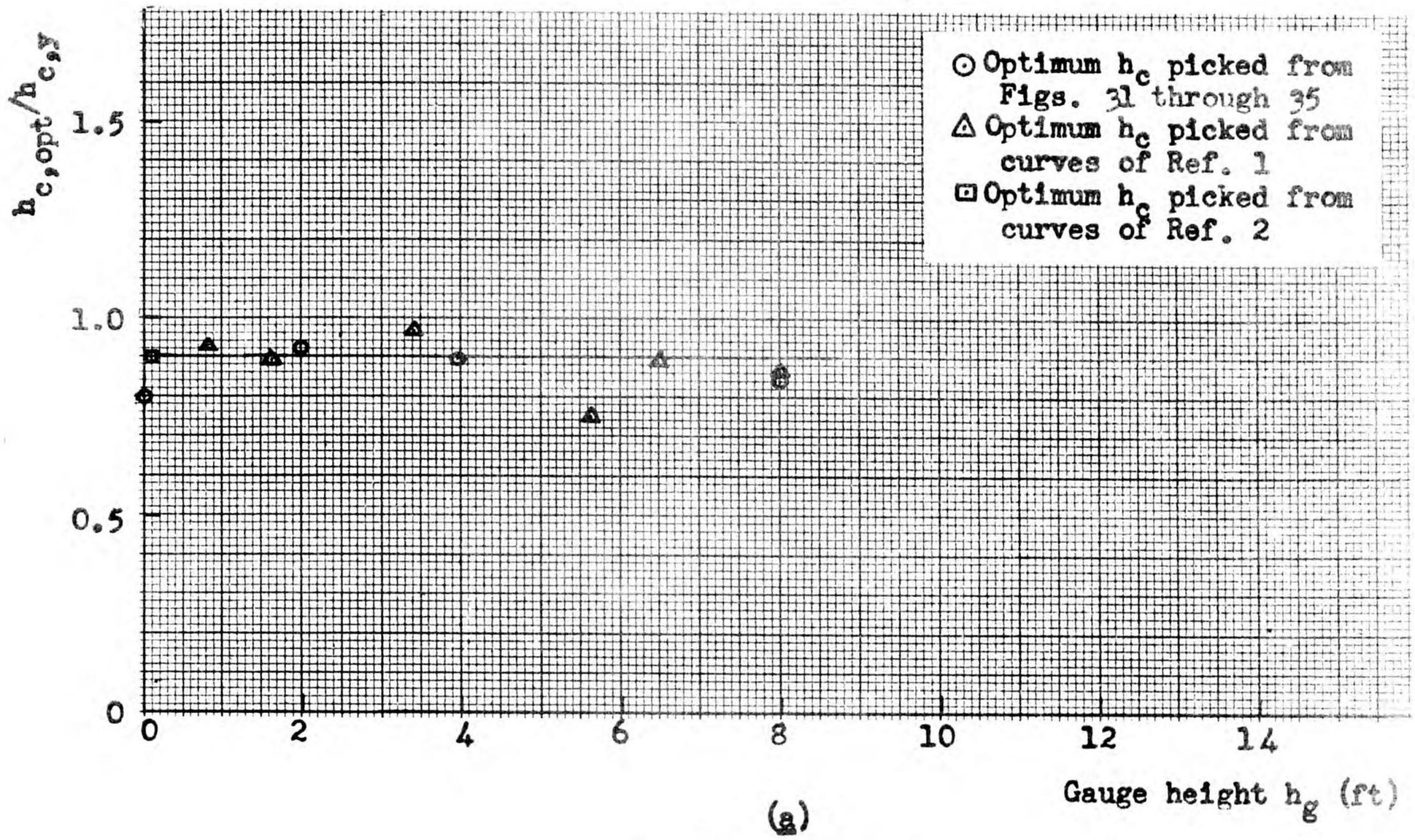

(a)

Averaged over h_g

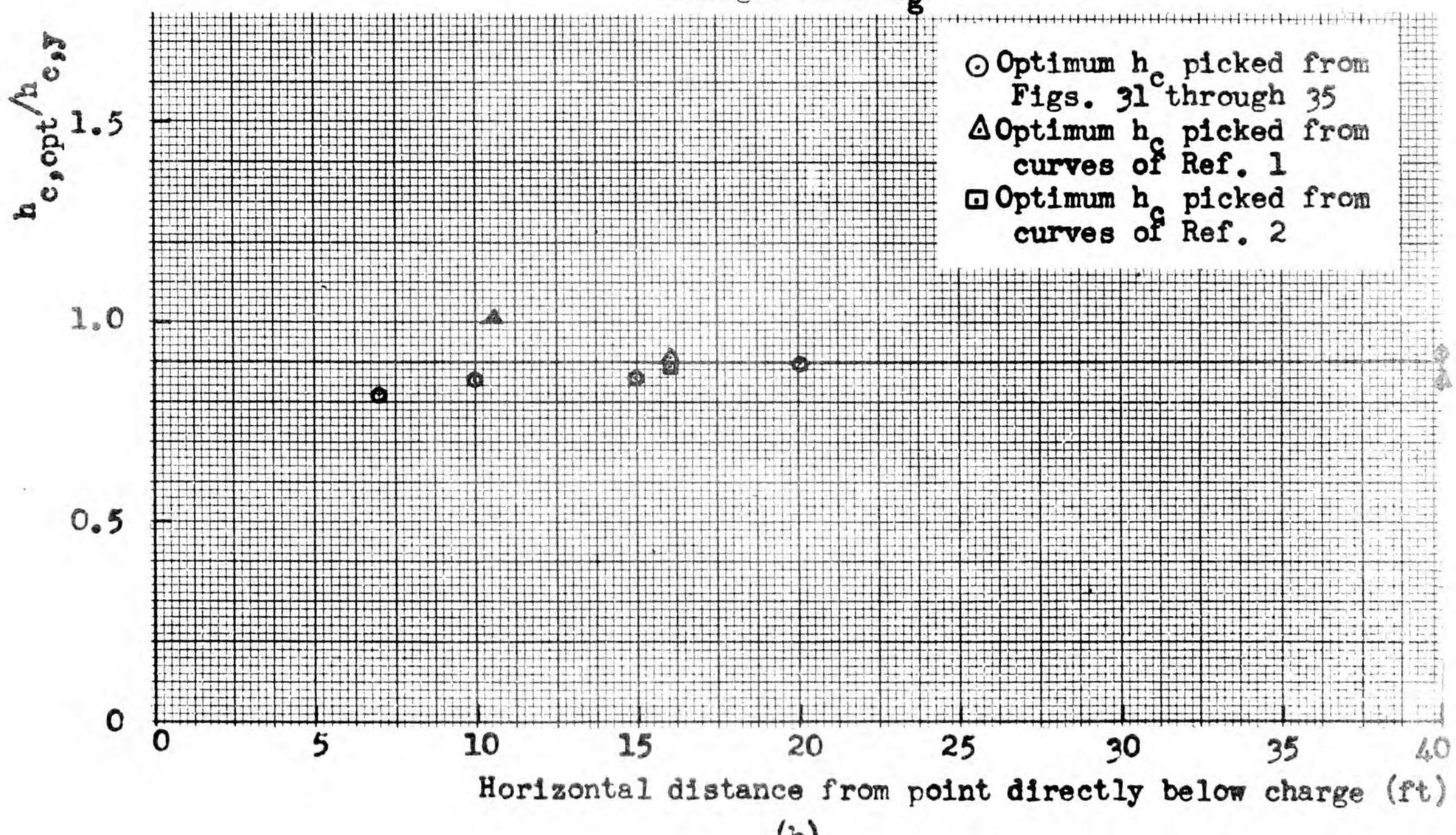

(b)

Fig. 36. Ratio of charge height to produce pressure maximum to that to produce triple point (a) versus gauge height, averaged over D; (b) versus horizontal distance from charge, averaged over h_g.

All units reduced to basis of 1 lb TNT.

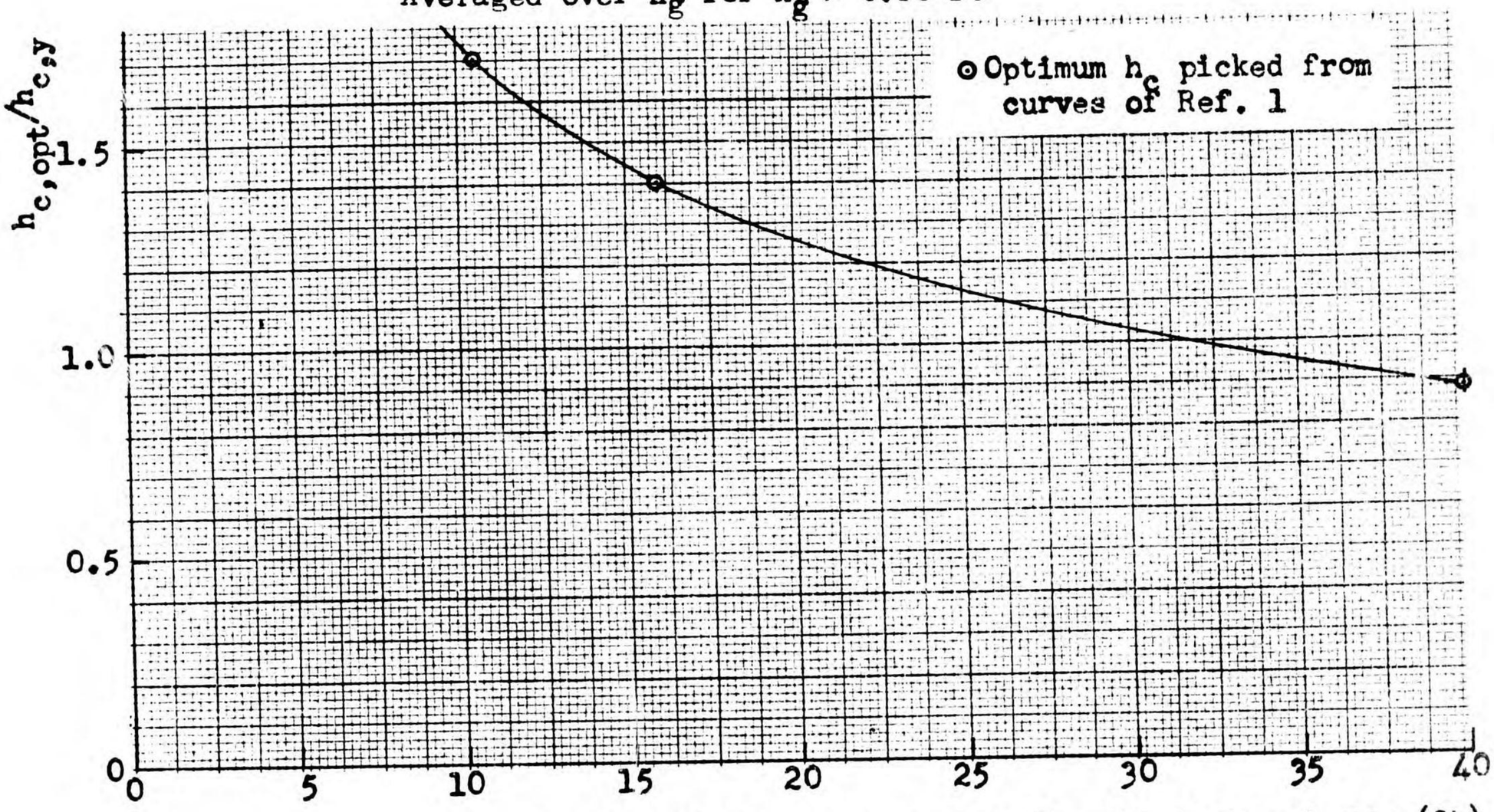

(a)

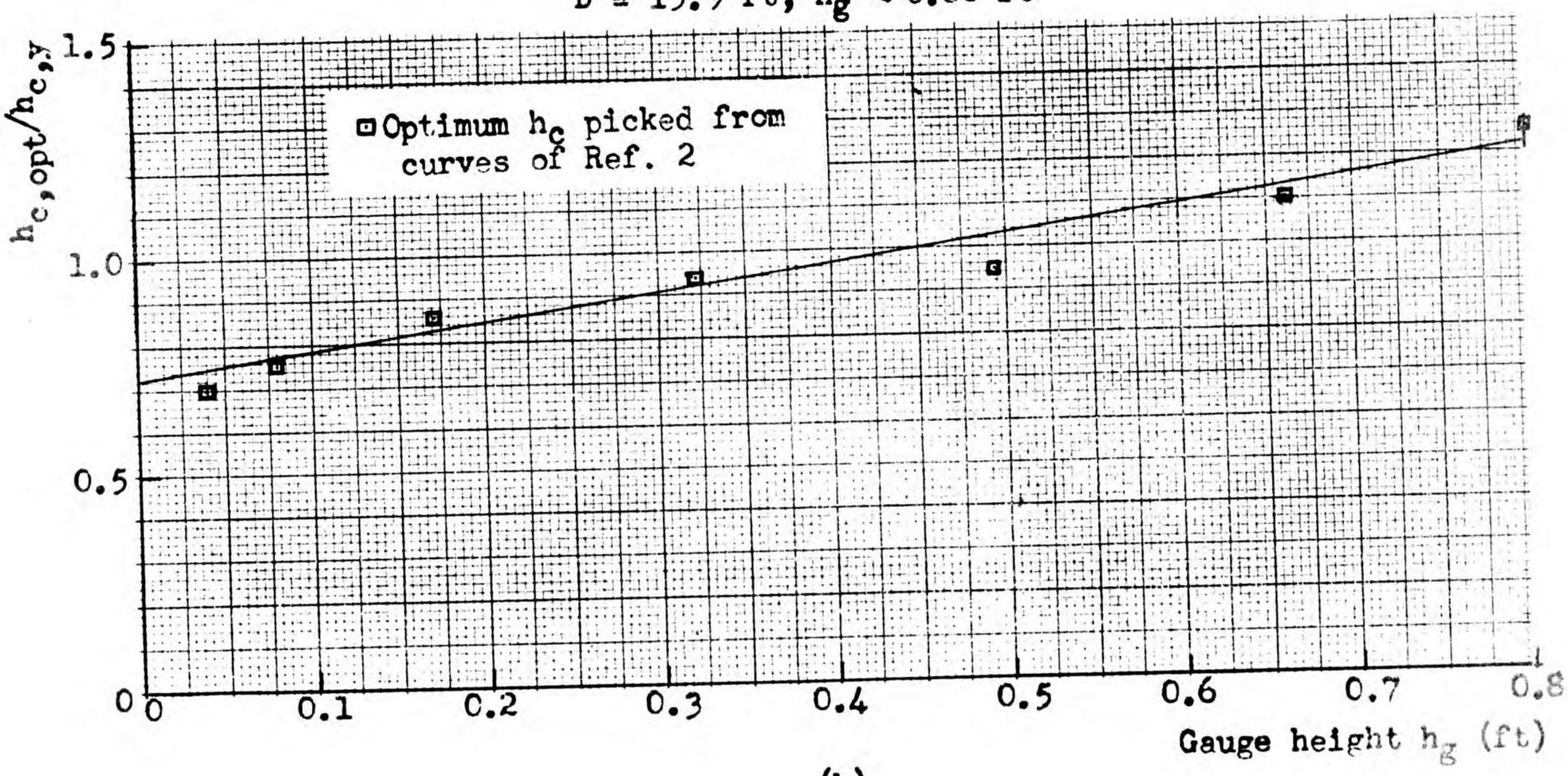

(b)

Fig. 37. Ratio of charge height to produce impulse maximum to that to produce triple point (a) versus horizontal distance from charge, averaged over h_g for h_g > 0.80 ft; (b) versus gauge height, D = 15.9 ft, h_g < 0.80 ft.

All units reduced to basis of 1 lb TNT.